

# **Design and optimization of new AgZnF<sub>3</sub>-based perovskite solar cells by using SCAPS-1D**

**A DISSERTATION REPORT  
SUBMITTED IN PARTIAL FULFILMENT OF THE REQUIREMENTS  
FOR THE AWARD OF DEGREE  
OF**

**MASTER OF SCIENCE  
IN  
APPLIED PHYSICS**

**Submitted by:**

**NISHANT  
(23/MSCPHY/56)  
SALIL CHAUDHARY  
(23/MSCPHY/57)**

**Under the Supervision of  
Dr. SARITA BAGHEL  
Assistant Professor**



**Department of Applied Physics  
DELHI TECHNOLOGICAL UNIVERSITY  
(Formerly Delhi College of Engineering)  
Shahbad Daultpur, Main Bawana Road, Delhi-110042, Delhi**

**June, 2025**



# DELHI TECHNOLOGICAL UNIVERSITY

(Formerly Delhi College of Engineering)  
Shahbad Daultapur, Main Bawana Road, Delhi-110042

## CANDIDATE'S DECLARATION

We NISHANT (23/MSCPHY/56) and SALIL CHAUDHARY (23/MSCPHY/57) of M.Sc. (Physics) hereby certify that the research work which is being presented in this thesis entitled “Design and optimization of new  $\text{AgZnF}_3$ -based perovskite solar cells by using SCAPS-1D ” which is submitted by us to the Department of Applied Physics, Delhi Technological University, Delhi in partial fulfilment of the award of the degree of Master of Science, is original and not copied from any source without proper citation.. This work has not previously formed the basis for the award of any Degree, Diploma Associateship, Fellowship or other similar title or recognition.

The matter presented in this thesis has not been submitted by me for the award of any other degree of this or any other Institute.

A handwritten signature in blue ink that reads "Nishant".

Nishant (23/MSCPHY/56)

A handwritten signature in blue ink that reads "Salil".

Salil Chaudhary (23/MSCPHY/57)

Date: June 06, 2025

Place: Delhi



# DELHI TECHNOLOGICAL UNIVERSITY

(Formerly Delhi College of Engineering)  
Shahbad Daultapur, Main Bawana Road, Delhi-42

## CERTIFICATE BY THE SUPERVISOR

I hereby certify that the project Dissertation titled “Design and optimization of new  $\text{AgZnF}_3$ -based perovskite solar cells by using SCAPS-1D” which is submitted by **Nishant** (23/MSCPHY/56) and **Salil Chaudhary** (23/MSCPHY/57), **Department of Applied Physics, Delhi Technological University**, Delhi, in partial fulfilment of the requirement for the award of the degree of Master of Science, is a record of the project work carried out by the students under my supervision. To the best of my knowledge this work has not been submitted in part or full for any Degree or Diploma to this University or elsewhere. The thesis embodies results of original work, and studies are carried out by the students themselves and the contents of the thesis do not form the basis for the award of any other degree to the candidate or to anybody else from this or any other University/Institution.

A handwritten signature in blue ink, which appears to read 'Dr. Sarita Baghel', is written over a horizontal line.

**Dr. Sarita Baghel**

**Assistant Professor,**

**Department of Applied Physics**

Date: June 06, 2025

Place: Delhi

## DECLARATION AND SUPERVISOR'S CERTIFICATE

We Nishant (23/MSCPHY/56) and Salil Chaudhary (23/MSCPHY/57) hereby certify that the work which is presented in the Dissertation-II entitled in fulfilment of the requirement for the award of the Master in Science in Physics and submitted to the Department of Applied Physics, Delhi Technological University, Delhi is an authentic record of our own, carried out during a period from January 2025 to May 2025 under the supervision of Dr. Sarita Baghel.

The matter presented in this report/thesis has not been submitted by us for the award of any other degree of this or any other Institute/University.

Title of paper: Design and optimization of new  $\text{AgZnF}_3$ -based perovskite solar cells by using SCAPS-1D

Author names (in sequence as per research paper): Nishant, Salil Chaudhary, Rahul kundara, Sarita Baghel

Have you registered for conference (Yes/No)?: NO

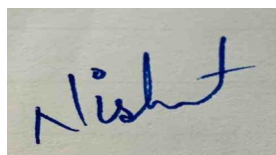
Status of paper (Accepted/Published/communication): Communication

Date of paper communication:

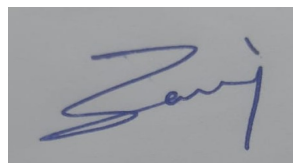
Date of paper acceptance:

Date of paper publication:

**Name (Roll No):**



Nishant (23/MSCPHY/56)



Salil Chaudhary (23/MSCPHY/57)

## **ACKNOWLEDGEMENTS**

We would like to express our deepest gratitude to Dr. Sarita Baghel, whose exceptional guidance and unwavering support have been crucial to the successful work of our M.Sc. dissertation. Her vast knowledge, insightful feedback, and constant encouragement were instrumental in shaping the direction of our research and significantly enhancing its quality. Dr. Baghel's dedication to her students' academic development has been an ongoing source of inspiration, and we are immensely thankful for the opportunity to learn under her mentorship.

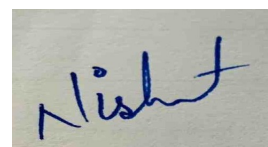
Our sincere thanks are also due to the Department of Applied Physics at Delhi Technological University, whose resources and infrastructure facilitated the smooth progression of our research work. The department's commitment to fostering a conducive academic environment and its emphasis on practical learning have been pivotal in our development as researchers.

We are also grateful to the esteemed faculty members and staff of the Department of Applied Physics for their invaluable assistance and insights throughout our academic journey. Their expertise and willingness to engage in meaningful discussions significantly enhanced our understanding of the subject and contributed to the overall quality of our work.

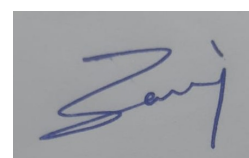
A special thanks goes to our fellow classmates and colleagues for their continuous support, collaboration, and stimulating discussions. Their input has played a key role in refining our research ideas and broadening our perspective.

In our research, we have made extensive use of the Solar Cell Capacitance Simulator one-dimensional program (SCAPS-1D), a powerful and open-source tool developed at the University of Gent, Belgium. This software, which accepts seven distinct semiconductor layers as input (excluding rear and front contacts), was invaluable in simulating the photovoltaic process. SCAPS-1D is an open-source, Windows-based tool for researchers in photovoltaic science and can be downloaded from the official website.

In conclusion, we extend our heartfelt thanks once again to Dr. Sarita Baghel and the Department of Applied Physics at Delhi Technological University for their invaluable guidance, support, and resources. Their contributions have been fundamental in the successful completion of our M.Sc. dissertation and have greatly shaped our academic journey.



NISHANT



SALIL CHAUDHARY

# **Design and optimization of new AgZnF<sub>3</sub>-based perovskite solar cells by using SCAPS-1D**

## **ABSTRACT**

The increasing energy demand globally, compounded by environmental concerns, is leading to the drive of renewable energy solutions which are cost effective, efficient and environmentally sustainable. The work investigated the potential of a new generation of AgZnF<sub>3</sub>-based PSC by comprehensively optimizing the electron transport layer (ETL), hole transport layer (HTL), absorber layer and other critical parameters such as thickness of absorber layer, defect density ( $N_t$ ), electron affinity, operating temperature, work function of back contact, series and shunt resistance using SCAPS-1D software. AgZnF<sub>3</sub>, absorber layer has suitable bandgap of 1.521 eV with superior holes and electrons mobility facilitates efficient photon and charge transfer yet minimum recombination losses. The device structure, FTO/ETLs/AgZnF<sub>3</sub>/HTLs/back contact, was systematically investigated by varying the ETLs, HTLs and back contacts to identify the optimized configuration. Among the various ETLs, WS<sub>2</sub> emerged the most appropriate ETL, while CBTS as HTL outperformed other HTLs by improving the charge extraction and minimizing loss due to recombination and exhibiting maximum efficiency for the device configuration of FTO/WS<sub>2</sub>/AgZnF<sub>3</sub>/CBTS/Au. The device obtained highest PCE of 31.77 % (with  $V_{OC}$  of 1.38 V,  $J_{SC}$  of 25.23 mA/cm<sup>2</sup> and FF of 90.82 %) at optimized value of different important parameters which effects the device performance as follows: thickness of absorber layer is 550 nm,  $N_t$  of 10<sup>14</sup> cm<sup>-3</sup> and at 300 K. These findings emphasize the importance of AgZnF<sub>3</sub>-based PSCs and highlights the critical need for its commercial application.

# **CONTENTS**

<b>Candidate's Declaration</b>	ii
<b>Certificate by the Supervisor</b>	iii
<b>Declaration and Supervisor's Certificate</b>	iv
<b>Acknowledgement</b>	v
<b>Abstract</b>	vi
<b>Contents</b>	vii-ix
<b>List of Figures</b>	x-xi
<b>List of Tables</b>	xii
<b>List of Symbols, abbreviations</b>	xiii - xiv
<b>CHAPTER 1 INTRODUCTION</b>	<b>1</b>
1.1 General	1
1.2 Research Objectives	2
1.2.1 Material Optimization	3
1.2.2 Device Structure Exploration	3
1.2.3 Active Layer Optimization	3
1.2.4 Stability and Efficiency Trade-offs	3
1.3 Significance	3
1.3.1 Development of Perovskite Solar Cells	3
1.3.2 Using less expensive back metal	3
1.3.3 Advancing through R&D	4
1.4 Working of Perovskite Solar Cell	4
<b>CHAPTER 2 LITERATURE REVIEW</b>	<b>6</b>

2.1 Perovskite Solar Cells	6
2.2 Basic Structure of Perovskite Solar Cells	6
2.3 AgZnF <sub>3</sub> Based Solar Cells	7
2.3.1 Crystal Structure of AgZnF <sub>3</sub>	8
2.3.2 Significance in Solar Energy Conversion	8
2.3.3 Optical Properties	9
2.3.4 Electrical Properties	9
2.4 Previous Research on AgZnF <sub>3</sub>	9
2.5 Properties of AgZnF <sub>3</sub>	10
2.6 SCAPS (Solar Cell Capacitance Simulator)	10
<b>CHAPTER 3 METHODOLOGY</b>	<b>13</b>
3.1 Material Selection and synthesis	13
3.2 SCAPS Simulation Setup	15
3.3 Device Architecture	16
3.3.1 AgZnF <sub>3</sub>	16
3.3.2 ETLs and HTLs	19
<b>CHAPTER 4 RESULTS AND DISCUSSIONS</b>	<b>20</b>
4.1 Calculation of different AgZnF <sub>3</sub> parameters for simulation	20
4.2 Exploring ETLs Variations	22
4.3 Exploring HTLs Variations	23
4.4 Thickness variation in Absorber Layer	25
4.5 Optimization of absorber layer defect density	26
4.6 Impact of electron affinity	27
4.7 Effect of operating temperature	28
4.8 Effect of work function of back contact	30



4.9 AC characterization	31
4.9.1 Impedance Spectroscopy (IS) measurement	31
4.10 Optical Absorption: Absorbance Coefficient vs Photon Energy	34
4.11 Effect of series resistance	36
4.12 Effect of shunt resistance	38
4.13 Practical insights drawn from simulation results	39
4.14 Verification with respect to the ideal Solar cell	41
4.15 Comparison of Simulation and Experimental Results	41
4.16 Challenges and Limitations	42
<b>CHAPTER 5 CONCLUSION</b>	<b>43</b>
<b>REFERENCES</b>	<b>44-45</b>

# **LIST OF FIGURES**

<b>CHAPTER 2</b>	<b>6</b>
Figure 2.1: Crystal structure of $\text{AgnF}_3$	8
Figure 2.2: SCAPS-1D simulation home window	12
Figure 2.3: SCAPS-1D simulation working window	12
 <b>CHAPTER 3</b>	
Figure 1.1: Device Architecture of $\text{AgZnF}_3$ -Based PSC	18
Figure 3.2: Band gap alignment of $\text{AgZnF}_3$ -based PSC	18
 <b>CHAPTER 4</b>	
Figure 4.1: J-V Characteristics of different ETLs	20
Figure 4.2: QE curves of different ETLs	20
Figure 4.3: J-V characteristics of different HTLs	21
Figure 4.4: QE plots of different HTLs	21
Figure 4.5: Band Diagram Analysis for ETLs	22
Figure 4.6: Band Diagram Analysis for HTLs	23
Figure 4.7: Impact of Variation in Thickness on PV Parameters	25
Figure 4.8: Impact of Variation in Defect Density on PV Parameters	27
Figure 4.9: Impact of Variation in Electron Affinity on PV	28
Figure 4.10: Impact of Variation in Temperature on PV Parameters	29
Figure 4.11: Graph of $J_{sc}$ vs Voltage of Different Back Metals	31

Figure 4.12: Graph of QE vs Wavelength of Different Back Metals	31
Figure 4.13: Nyquist Plot of Impedance for ETLs with different CBO values	33
Figure 4.14: Nyquist plot of Impedance Response for HTLs with different VBO values	34
Figure 4.15: Variation of Absorption Coefficient with Photon Energy for absorber layer and various ETLs.	35
Figure 4.16: Variation of Absorption Coefficient with Photon Energy for various HTLs.	36
Figure 4.17: Effect of Series Resistance on PV Performance	37
Figure 4.18: Effect of Shunt Resistance on PV Performance	39
Figure 4.19: J-V Characteristics for FTO/WS <sub>2</sub> /AgZnF <sub>3</sub> /CBTS/Au Photovoltaic Device.	41
Figure 4.20: Q.E. vs Wavelength Characteristics for FTO/WS <sub>2</sub> /AgZnF <sub>3</sub> /CBTS/Au Photovoltaic Device.	40

# **LIST OF TABLES**

## **CHAPTER 3**

Table 3.1 Simulation parameters of various ETLs	19
Table 3.2 Simulation parameters of various HTLs	19

## **CHAPTER 4**

Table 4.1 Comparative analysis of Photovoltaic (PV) Parameters of AgZnF <sub>3</sub> based PSC	24
Table 1.2 Performance Parameters of Photovoltaic Device with different Back Metals.	30
Table 4.3. CBO and VBO values For AgZnF <sub>3</sub> -based PSC	32

## **LIST OF SYMBOLS**

<b>SYMBOL</b>	<b>Description</b>
<b>J<sub>SC</sub></b>	Short Circuit Current
<b>V<sub>OC</sub></b>	Open-Source Voltage
<b>E<sub>g</sub></b>	Bandgap
<b>N<sub>C</sub></b>	Effective Density of States in Conduction band
<b>N<sub>V</sub></b>	Effective Density of States in Valence band
<b>N<sub>D</sub></b>	Concentration of Donor impurities
<b>N<sub>A</sub></b>	Concentration of Acceptor impurities
<b>χ (eV)</b>	Electron Affinity
<b>ε<sub>r</sub></b>	Dielectric Constant
<b>V<sub>e</sub> (cm/s)</b>	Thermal Velocity of Electrons
<b>V<sub>h</sub> (cm/s)</b>	Thermal Velocity of Holes
<b>μ<sub>n</sub> (cm<sup>2</sup>/Vs)</b>	Electron Mobility
<b>μ<sub>h</sub>(cm<sup>2</sup>/Vs)</b>	Hole Mobility
<b>N<sub>t</sub> (cm<sup>-3</sup>)</b>	Defect Density

## **LIST OF ABBREVIATIONS**

<b>SYMBOL</b>	<b>Description</b>
<b>PV</b>	Photovoltaic
<b>PSC</b>	Perovskite Solar Cell
<b>FF</b>	F.F.

<b>QE</b>	Quantum Efficiency
<b>PCE</b>	Power Conversion Efficiency
<b>HTL</b>	Hole Transport Layer
<b>ETL</b>	Electron Transport Layer
<b>SCAPS-1D</b>	Solar Cell Capacitance Simulator 1-D
<b>FTO</b>	Fluorine-doped Tin Oxide
<b>CBO</b>	Conduction Band Offset
<b>VBO</b>	Valence Band Offset
<b>R<sub>s</sub></b>	Series Resistance
<b>R<sub>SH</sub></b>	Shunt Resistance
<b>IS</b>	Impedance Spectroscopy

# **CHAPTER 1**

## **INTRODUCTION**

Energy is one of the primary aspects that contribute to forming the world we live in because it propels almost every aspect of life and society[1–3]. Far beyond mere convenience, it is an indispensable foundation for survival, giving essential services like heating, lighting, food security, climate control, all critical to health, safety and equitable for survival [4]. It is the lifeblood of modern life. As population is growing with much faster rate exceeding the historical average of 2 %, the demand for energy continues to escalate. Enhanced lifestyle and the demand of the energy are rising together in the same manner[1]. Higher energy demand, especially from fossil fuels such as coal, oil, natural gases like methane etc., results in a rise in greenhouse gas emissions which leads to global warming, glaciers melting and climate variability, increasing ocean levels, water pollution and air pollution, ozone depletion and forest degradation which results in severe droughts and floods and leads to disasters[1,5]. Thus, the need for the renewable energy source becomes critical to fulfil the increasing demand of energy. One solution to deal with this problem and energy shortage is to expand the renewable energy sources use and adopt new technologies. It is therefore to choose the eco-friendly energy sources for the improvement of the future world[6]. Renewable energy's critical importance stems from its transformative potential to deliver sustainable, cost effective and environmentally friendly as a replacement to finite, polluting fossil fuels. Unlike coal, oil, or other non-renewable energy sources, renewable resources like solar power produce electricity by having no emission of detrimental greenhouse gases, making them an indispensable tool for alleviating climate change and limiting air pollution.

Among renewable energy resources, solar energy excels as the most prolific energy resource. The sun radiates energy at an astonishing rate of nearly  $10^{23}$  kilowatt, with approximately  $10^{14}$  kilowatt is captured by earth. Much of energy from solar power is not used and is basically wasted and as the solar energy arrives on earth in multiple forms, including light and heat, thus this energy should be utilized by us for our own good[7]. We can use this energy by the help of developing solar cells, which are the devices designed to transform the energy from sunlight (light energy) into electrical energy with the help of photovoltaic technology. Solar technology is so versatile, capable of being deployed at both small and large scales. Solar energy solutions exhibit remarkable versatility, spanning from the residential and corporate rooftops installations to large scale solar farms in sun rich regions, provisioning a wide array of energy demands. Solar cells, commonly referred as Photovoltaic (PV) cells, which is an oblique combination of two words, “photo” and “voltaic”, meaning “light” and “electricity”, respectively. It directly converts sunlight into electricity power.

Though silicon solar cells are widely commercialized, their manufacture is costly, energy-intensive, and is not so efficient. Also, they tend to be brittle, require a large surface area, and create environmental hazard as disposed of. Therefore, new PV materials are actively sought to either surpass the efficiency limits of the silicon (Si) PV without escalating costs or to seamlessly integrate with Si technology as low-cost, high-performance enhancers. As a result, we are moving toward more sophisticated absorbing materials with larger absorption coefficients, which enable better absorption of solar light and improve solar cell efficiency.

In recent years, PSCs (perovskite solar cells) has risen as a generational photovoltaic technology offering transformative potential for high efficiency, flexibility and low-cost renewable energy solutions. These cells utilize hybrid organic-inorganic materials, usually Pb or tin halides as the active

light absorbing layers. Since their inception in 2009, when Miyasaka's team achieved a modest 3.8% [8] efficiency using perovskite in a dye sensitized configuration, advancements have been meteoric, with lab scale efficiencies now exceeding 26.1% [9], rivalling standard silicon-based solar cells.

Initially, perovskite photovoltaic cells based on lead have revolutionized photovoltaics with the record efficiencies exceeding 23% [10–12], which is close to silicon. Also, Pb-based halide perovskites have exhibit PCE of around 29.1% [12] but, despite their promise, challenges persist. Long-term operational stability when exposed to environment have been the major issue for lead based solar cells. Environmental factors like moisture, heat, ultraviolet radiation exposure and issues with the lead toxicity and less availability necessitate urgent research into encapsulation strategies and lead-free alternatives like tin-based perovskites [13] or germanium-based perovskites [14] or others, which have low toxicity and more environmentally friendly. Among them, Sn holds the most promise because of the remarkable properties of Sn-based perovskite material that includes excellent charge carrier mobility, extended carrier lifetimes and optimal of 1.3-1.4 eV, matching closely to the Shockley-Quiser limit for solar energy conversion [15]. A major issue with Sn-based PSCs is that Sn rapidly oxidises to  $\text{Sn}^{4+}$  (from  $\text{Sn}^{2+}$ ), which occurs quickly under normal environmental conditions. This oxidation causes the perovskite material to degrade, leading to decline in the durability and efficiency [12]. The basic design of the PSCs is typically organized into functional layers that work collaboratively to absorb sunlight, separate charges and transport the electrons and holes to produce electricity. Layers sandwiched between the electrodes there are charge transport layers, which includes layer that transport electrons, typically metal oxides and the layer that transport holes, which might use organic materials like PEDOT: PSS, Spiro-OMeTAD or inorganic compounds like NiO,  $\text{Cu}_2\text{O}$ , CuI [16,17]. At the core lies perovskite absorber layer, a crystalline material with the general formula  $\text{ABX}_3$  [8].

There are excellent choices for the photovoltaic perovskite materials. Silver zinc fluoride ( $\text{AgZnF}_3$ ) has emerged as standout candidate among high-performance perovskite materials for photovoltaics [18]. By leveraging the unique chemistry of  $\text{Ag}^+$  and  $\text{Zn}^{2+}$  cations in a fluoride matrix,  $\text{AgZnF}_3$  combines the benefits lead-free composition, structural stability and tuneable electronic properties.  $\text{AgZnF}_3$  exhibits a bandgap of 1.521 eV making it an excellent contender for use in PSCs [18]. Also, recent studies reveal its exceptional thermoelectric performance, achieving ZT value (dimensionless figure of merit) of 2.56 at 1200 K and a thermoelectric conversion efficiency of 37 %, positioning it as a candidate for thermal energy recycling technologies [19]. In this work, we have optimized  $\text{AgZnF}_3$ -based perovskite solar cells by varying different ETLs and HTLs in order to identify the configuration which gives the maximum performance. After optimizing device structure, fundamental parameters like defect concentration, absorber layer thickness, work function of back contact, operating temperature, series and shunt resistance were analysed to further enhance photovoltaic performance. The device's performance was analysed using SCAPS-1D simulation software by analysing the key parameters which are power conversion efficiency, short-circuit current density ( $J_{\text{sc}}$ ), open circuit voltage ( $V_{\text{oc}}$ ), and fill factor (FF). SCAPS-1D provides theoretical framework for a device. The  $V_{\text{oc}}$  is determined by the alignment of fermi energy levels between electron transport layer and hole transport layer, whereas the  $J_{\text{sc}}$  and FF increases with increase in charge mobility of ETL [20]. Simulation results demonstrates that  $\text{AgZnF}_3$ -based PSC exhibits improved thermal resilience and high efficiency of 31.77 % with  $V_{\text{oc}}$  of 1.38 V,  $J_{\text{sc}}$  of 25.23  $\text{mA}/\text{cm}^2$  and FF of 90.82 % at 300 K. Its favourable electronic properties and performance metrics position it as a highly potential photovoltaic material for applications in future.

## 1.2 Research Objectives:

The work objective is to explore and optimize the performance of perovskite solar cells (PSCs) using SCAPS-1D simulation software. And The focus is on the application of the fluoroperovskite material  $\text{AgZnF}_3$  as the absorber layer. The research aims to enhance the efficiency, stability, and overall



performance of PSCs through material and structural optimization, performance evaluation, and stability analysis under varying environmental conditions.

This includes –

### **1.2.1 Material Optimization**

The simulation is done by using Solar Cell Capacitance Simulator (SCAPS-1D) simulation software. The active layer used is the perovskite material  $\text{AgZnF}_3$ . Simulations are conducted using SCAPS-1D to analyse how changes in key parameters such as the bandgap, carrier mobility, and recombination rates affect photovoltaic efficiency. Using the simulation software, investigate how variations in the material properties of the perovskite  $\text{AgZnF}_3$  affect the overall performance of perovskite solar cells. This will identify the ideal material properties for maximum light absorption and charge transport.

### **1.2.2 Device Structure Exploration**

Study the impact of different structures of the devices, by varying the thickness of the perovskite layer, using a different electron transport layer and hole transport layers, and varying their respective doping levels affect device performance.

Optimization of these parameters will minimize the recombination losses and further improve the efficiency and stability of the devices.

This study will identify the optimal ETL and HTL combinations for achieving high-performance, stable perovskite solar cells.

### **1.2.3 Active Layer Optimization**

The performance of  $\text{AgZnF}_3$ -based fluoroperovskite solar cell is evaluated by simulating the performance metrics, such as open-circuit voltage ( $V_{oc}$ ), short-circuit current ( $J_{sc}$ ), fill factor (FF), and power conversion efficiency (PCE) under various conditions. This will give insights into how different structural and material will influence the performance of the device.

### **1.2.4 Stability and Efficiency Trade-offs**

To assess trade-offs between efficiency and stability of perovskite solar cells under different environmental factors, including temperature and light intensity, for designing highly durable, high-performance devices to be suitable for real-world applications.

## **1.2 Significance**

### **1.3.1 Development of Perovskite Solar Cells**

Perovskite solar cells demonstrated their potential to surpass the efficiency of traditional silicon-based solar cells. Perovskites offer advantages such as a broader absorption spectrum, which allows them to capture more sunlight, and better charge-carrier mobility, which leads to higher efficiency.

### **1.3.2 Using less expensive back metal contact**

We can use stable metal contacts like nickel, which has a bandgap of approximately 5.04 eV and Pd which has a Band Gap of 5.6 eV that offers good efficiencies in comparison to with the gold and silver, and platinum. Although Gold and Silver are widely used as back metal contacts in simulation.

### 1.3.3 Advancing through Research and Development

Even if not yet widely applied,  $\text{AgZnF}_3$  is not a widely studied material. It could serve as a research tool to explore fluoride-based materials in inorganic chemistry, solid-state physics, and material engineering. Researching its synthesis, stability, and reactivity could provide insights into broader applications for similar compounds in specialized fields of science.

## 1.4 Working of Perovskite Solar Cells

The basic principle of the perovskite solar cell is the process of turning light energy, which are photons into electrical energy and this effect is known as photovoltaic effect.

Creation of the Electron-Hole a-pairs –

When the solar cell is exposed to sunlight, photons from the sunlight strike on the surface of the solar cells and are absorbed by the semiconductor material or the perovskite material (The working principle of perovskite-based solar cells is much like a traditional photovoltaic cell, but the difference comes with the benefit of a perovskite-structured material that can serve as the light-absorbing layer). This will excite the electrons and creates electrons and hole pairs.

Separation of the Charges –

The excited electrons move to the conduction band while the holes stay in the valence band. by this there is a splitting of the electrons and holes quasi fermi levels  $E_{Fn}$  and  $E_{Fp}$

Flow of Current –

The charges which are separated moved under the influence of the electric field inside the solar cell. The electrons move towards the front surface of the cell while the holes move towards the rear surface of the cell. The moving electrons and holes are caught by the metal contacts of the front and back surfaces of the cell by which electric current is produced. But, contact selectivity is achieved not only due to the presence of an electric field but can be obtained by a preferential kinetic exchange at one of the selective contacts of the carriers of one kind while keeping the other kind blocked and the process of light absorption by a layer of dye molecules injecting electrons selectively into the conduction band of a semiconductor while blocking holes due to band alignment. A similar process injects holes into a hole-transporting material. The electrons release an electrical current.

Efficiency –

The efficiency of the solar cell in photoconversion can be determined by the product of three photovoltaic parameters: Photocurrent, photovoltage, and the fill factor. The maximum photocurrent is the one which is usually limited by the bandgap of the material absorbing the light but the photocurrent also gets reduced by non-optimum charge collection.

In dark conditions with no applied bias the Fermi level,  $E_{FO}$ , equilibrates all around the device.

Build in potential  $V_{bi}$

Because the n-doped and p-doped layers have low and high work functions, respectively, equilibration creates a built-in potential,  $V_{bi}$ . The bands of the light-absorbing layer, being intrinsic in

nature, are leaned along its entire thickness by an electrical field in that intrinsic region. In the region, drift current plays the major determining role regarding charge separation and collection.

#### Open-Source Voltage $V_{OC}$ –

This separation of Fermi levels leads to flat band conditions, which cancel the electrical field, thus annulling the collection driving force for the photocurrent. The model's  $V_{oc}$  is, therefore, limited by work functions of the contacts. This model was used to explain the  $V_{oc}$  in amorphous Si solar cells and was originally used for organic solar cells. [27]

#### Circuit of Solar Cell –

A Solar Panel is mad of parallel or series arrangement of solar cells. The electrical energy produced can be fed into the grid, and can be stored in batteries and other storing devices and can be utilized.

# **CHAPTER 2**

## **LITERATURE REVIEW**

### **2.1 Perovskite Solar Cells**

Perovskite solar cells are the Solar Cells that uses perovskite materials to produce electricity when exposed to sunlight. Perovskite materials have a specific crystal structure with the formula  $ABX_3$  where, (X = oxygen, halogen) and (A is cation and B is Anion). The larger A cation occupies a cubo-octahedral site, which is shared with twelve X anions, while the smaller B cation is stabilized in an octahedral site, shared with six X anions. When light hits the Perovskite material it absorbs photons and excite electrons and create electron-hole pairs. The excited electrons move through the electron transport layer (ETL), and the holes move through the hole transport layer (HTL). And the electrons reach to the cathode and the holes reach the cathode, creating a flow of the electricity. The flow of charge is harnessed as Direct Current (DC)

The Perovskite Materials are used as an active layer for gathering light and the absorbing layer is usually an organic or inorganic halides. Perovskite solar cells demonstrated their potential to surpass the efficiency of traditional silicon-based solar cells. Perovskites offer advantages such as a broader absorption spectrum, which allows them to capture more sunlight, and better charge-carrier mobility, which leads to higher efficiency.

The performance of perovskite solar cells is highly dependent on the quality and properties of the electron transport layers (ETLs) and hole transport layers (HTLs). These layers serve as intermediaries to extract and transport the electrons and holes generated by the solar cell. Studies have focused on optimizing these materials for improved charge extraction, reduced recombination losses, and enhanced stability. Materials like Titanium Dioxide ( $TiO_2$ ) and PCBM are often used for ETLs, while Spiro-OMeTAD and CuSCN are examples of HTLs used in PSCs.

### **2.2 Basic Structure of Perovskite Solar Cells**

The perovskite Solar Cell consists of many layers that collaborate to transform sunlight into electrical energy.

- Substrate

The substrate is the base layer, which is typically made of glass, plastic, or metal. substrate provides mechanical support for the entire solar cell structure

- Transparent conductive Layer (TCO)

The TCO is a transparent, conductive layer that allows light to pass through while conducting electrons. Common materials include indium tin oxide (ITO) and fluorine-doped tin oxide (FTO).

- Electron Transport Layer (ETL)

ETL is placed between the perovskite layer and the TCO. Its main role is to transfer the excited electrons from the perovskite layer to the anode. The most common materials used for the ETL are  $\text{TiO}_2$  (titanium dioxide),  $\text{SnO}_2$  (tin oxide). It also prevents holes from reaching the cathode, thereby ensuring efficient charge separation.

- Perovskite Layer

The Perovskite layer also known as light-absorbing is the most important part of the perovskite solar cell. The perovskite material is generally a compound with the formula  $\text{ABX}_3$ , where A is an organic cation, B is a metal cation, and X is a halide anion. It absorbs sunlight and generates electron-hole pairs when exposed to light.

- Hole Transport Layer (HTL)

The HTL layer supports hole transport - that means transporting positive charge carriers or holes from the perovskite layer to the cathode. This layer most often uses a material such as spiro-OMeTAD (a hole-transporting organic material), or NiO (nickel oxide) and other materials

- Top Electrode (Cathode)

The top electrode, or cathode, is typically composed of conductive metals such as gold (Au), silver (Ag), or tungsten (W). This layer collects the electrons that have traveled through the ETL and transports them to the external circuit. The choice of metal affects not only the device's efficiency but also its cost and stability, particularly under operational conditions.

- Back Electrode (Anode)

The back electrode, or anode, is often constructed from the same transparent conductive materials used in the TCO layer, such as ITO or FTO. It collects the holes transported through the HTL and plays a vital role in completing the circuit

Through the transparent conductive oxide layer the sunlight enters into the solar cell and this light is absorbed by the perovskite layer. This absorption of light produces pairs of electron and holes. Holes flow towards the hole transport layer and electrons flow towards the electron transparent layer. Then the holes are gathered by the Back Electrode which is anode and the electrons are gathered by the top Electrode which is cathode, producing an electrical light and generates current.

## 2.3 $\text{AgZnF}_3$ Based Solar Cells

### 2.3.1 Crystal Structure of AgZnF<sub>3</sub>

The density function theory (DFT) with GGA and PBE was employed to determine the structural, electrical, and optical properties of pure doped AgZnF<sub>3</sub> type Fluro-perovskite. The structural properties are calculated in realistic agreement with those testified in the literature. The band gap of the hybrid AgZnF<sub>3</sub> is 1.52 eV. [19]

The crystal structure of AgZnF<sub>3</sub> (Silver Zinc Fluoride) belongs to the perovskite structure, which is a well-known type of crystal lattice. Specifically, it adopts a pseudo cubic perovskite structure.

- ❖ In this structure, the general formula for a perovskite is ABX<sub>3</sub>, -
- ❖ A represents a larger cation (in this case, Ag<sup>+</sup> for silver)
- ❖ B represents a smaller cation (here, Zn<sup>2+</sup> for zinc)
- ❖ X represents an anion (in this case, F<sup>-</sup> for fluoride)

The elemental configuration for considered atoms is: silver (Ag): 1s<sup>2</sup> 2s<sup>2</sup> 2p<sup>6</sup> 3s<sup>2</sup> 3p<sup>6</sup> 3d<sup>10</sup> 4s<sup>2</sup> 4p<sup>6</sup> 4d<sup>10</sup>, zinc (Zn): 1s<sup>2</sup> 2s<sup>2</sup> 2p<sup>6</sup> 3s<sup>2</sup> 3p<sup>6</sup> 4s<sup>2</sup> 3d<sup>10</sup>, fluorine (F): 1s<sup>2</sup> 2s<sup>2</sup> 2p<sup>5</sup>. A large part of Fluoride Perovskites materials such as AgZnF<sub>3</sub> have a cubic structure at room temperature. When the energy of crystals was low, the equilibrium lattice constant was estimated using the Monahan equation of state, and the results were calculated for suitable lattice constant values. [19]

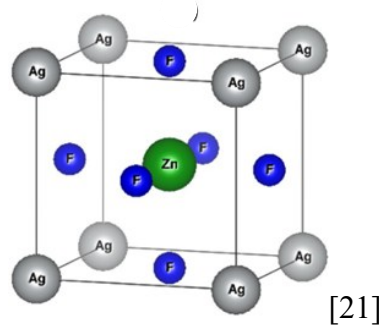


**Figure 2.1:** Crystal structure of AgZnF<sub>3</sub>

- ❖ The crystal structure of AgZnF<sub>3</sub> is typically described as -
- ❖ Ag<sup>+</sup> ions are located at the corners and the centre of a cubic unit cell, forming a cubic lattice.
- ❖ Zn<sup>2+</sup> ions are positioned at the face centres of the unit cell.
- ❖ F<sup>-</sup> ions occupy the positions between these metal cations in a fluorite-like arrangement.

### 2.3.2 Significance in Solar Energy Conversion

High Photovoltaic Efficiency Potential - Photovoltaic efficiency refers to how effectively a material can convert sunlight into electrical energy. The higher the efficiency, the more sunlight a material can convert into usable electricity.

Perovskite solar cells have gained significant attention due to their remarkable efficiency, ease of fabrication, and low cost. Materials like AgZnF<sub>3</sub>, with a perovskite-like structure, could be

explored as alternative light-absorbing materials, with the potential to offer competitive efficiencies in photovoltaic devices.

The  $\text{AgZnF}_3$  structure have favourable optical properties for light absorption, which is crucial for any material used in solar cells.

**Stability and Durability –**

Stability and durability are crucial for the long-term performance of solar cells. Perovskite solar cell technology is the stability of the materials, especially under harsh environmental conditions (such as exposure to moisture, UV radiation, and high temperatures).

$\text{AgZnF}_3$  exhibits strong covalent bonds and a weak ionic character.

**Bandgap Engineering -** Bandgap engineering refers to the process of adjusting the energy gap (the bandgap) between the valence band (where electrons are bound) and the conduction band (where electrons are free to move and conduct electricity) of a material.

$\text{AgZnF}_3$  have a bandgap of around 1.1 to 1.5 eV is ideal for efficient light absorption in solar cells.

### **2.3.3 Optical Properties**

The electronic polarizability of material is revealed through the actual portion of the dielectric function  $\epsilon_1(\omega)$ . The zero-frequency limit  $\epsilon_1(0)$  of  $\text{AgZnF}_3$  is 2.9.  $\text{AgZnF}_3$  has a greater band gap than other compounds, and since  $\epsilon_1(0)$  is less for the former than the latter, it follows that  $\epsilon_1(0)$  varies inversely with band gap for this compound. [19]

### **2.3.4 Electrical Properties**

$\text{AgZnF}_3$ 's total electronic properties are principally controlled by the Zn atom, whereas the Zn-d state and the F-p state had a minor impact on its partial electronic properties and state density. Cu doping modified  $\text{AgZnF}_3$  electrical band structure by narrowing the band gap. With increasing doping concentrations, the partial densities of states, which are likewise impacted by doping concentrations decreased. [19]

The electrical properties of  $\text{AgZnF}_3$  (Silver Zinc Fluoride) are influenced by its perovskite-like crystal structure.

## **2.4 Previous Research on $\text{AgZnF}_3$**

There is no experimental work on the perovskite material  $\text{AgZnF}_3$  till now for the solar cell. However, there is limited direct experimental research work on  $\text{AgZnF}_3$  (Argentum Zinc Fluoride) for use in solar cells.

This material is more often studied in the context of photonics, optical properties, and electronic applications.

## 2.5 Properties of AgZnF<sub>3</sub> (argentum zinc fluoride)

The key Properties of AgZnF<sub>3</sub> used in the simulation work are –

**Bandgap - 1.52**

**Electron Affinity – 4.0**

**Dielectric Permittivity – 2.9**

**CB Density of states –  $7.579 \times 10^{18}$**

**VB Density of states –  $4.026 \times 10^{19}$**

**Electron Thermal Velocity –  $1 \times 10^7$**

**Hole Thermal Velocity –  $1 \times 10^7$**

**Electron Mobility - 695**

**Hole Mobility - 27**

**Uniform Donor Density - 0**

**Uniform Acceptor Density –  $6.260 \times 10^{20}$**

## 2.6 SCAPS (Solar Cell Capacitance Simulator)

SCAPS (a Solar Cell Capacitance Simulator) is a one-dimensional open-source solar cell simulation programme developed at the Department of Electronics and Information Systems (ELIS) of the University of Gent, Belgium. The was originally programme is developed for cell structures of the CuInSe<sub>2</sub> and the CdTe family. Recent developments make the programme now also applicable to crystalline solar cells (Si and GaAs family) and amorphous cells (a-Si and micromorphous Si).

It offers a platform for evaluating and improving the optical and electrical characteristics of different kinds of photovoltaics encompassing and not limited to perovskite, thin-film, and silicon-based solar cells. SCAPS-1D simulates solar cell dynamics through the use of numerical methods.

The most recent version, SCAPS 3.8, includes,

- Study up to 7 semiconductor layers
- almost all parameters can be graded (i.e. dependent on the ocal composition or on the depth in the cell): *E<sub>g</sub>, chi, epsilon, N<sub>c</sub>, N<sub>v</sub>, V<sub>thn</sub>, V<sub>the</sub>, μ<sub>n</sub>, μ<sub>p</sub>, N<sub>A</sub>, N<sub>D</sub>*, all defects *N<sub>t</sub>*
- recombination mechanisms: band-to-band (direct), Auger, SRH-type
- contacts: work function or flat-band; optical property (reflection of transmission filter) filter
- tunnelling: intra-band tunnelling (within a conduction band or within a valence band); tunnelling to and from interface states



- illumination: from either the  $p$ -side or the  $n$ -side; spectrum cut-off and attenuation
- working point for calculations: voltage, frequency, temperature
- defect levels, optical property: direct excitation with light possible (impurity photovoltaic effect, IPV)
- the programme calculates energy bands, concentrations and currents at a given working point,  $J$ - $V$  characteristics, ac characteristics ( $C$  and  $G$  as function of  $V$  and/or  $f$ ), spectral response (also with bias light or voltage)
- batch calculations possible; presentation of results and settings as a function of batch parameters
- loading and saving of all settings; startup of SCAPS in a personalised configuration; a script language including a free user function.

Researchers who have contributed to its development:  
 Alex Niemegeers, Marc Burgelman, Koen Decock, Stefaan Degrave, Johan Verschraegen.

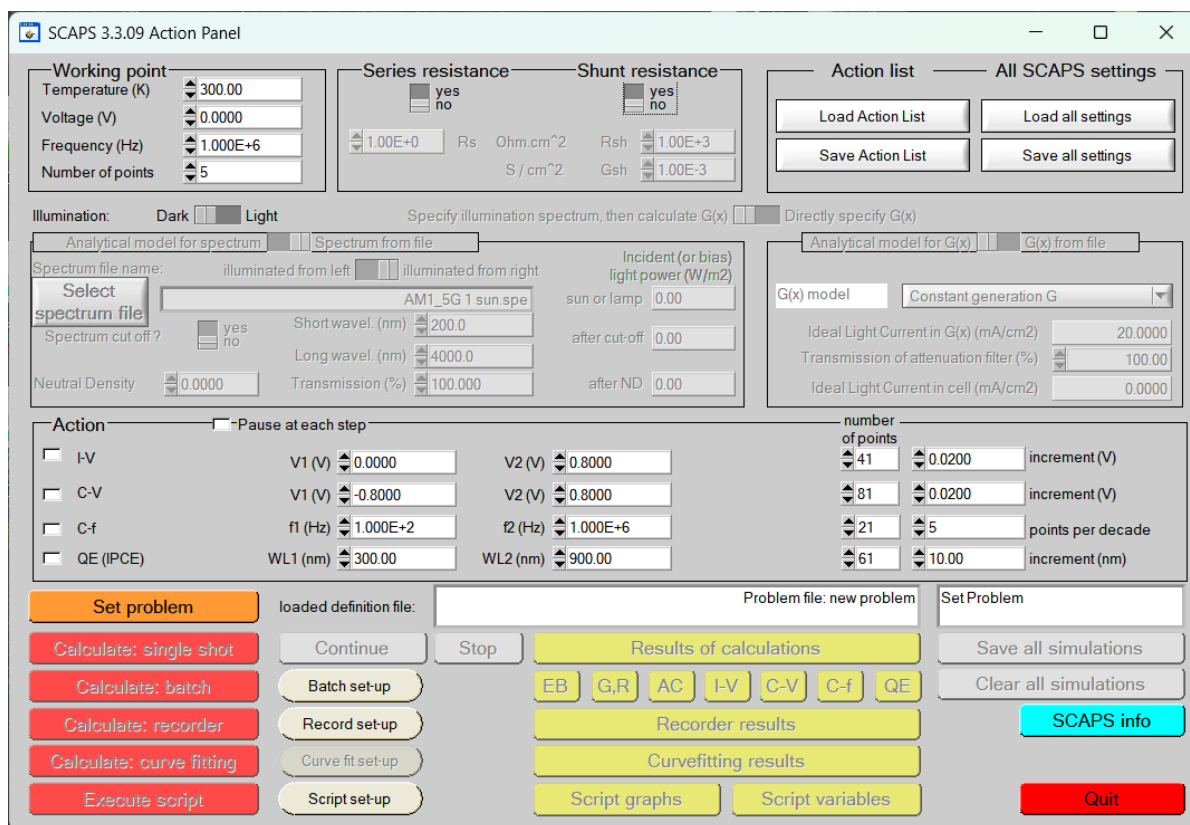


Figure 2.2: SCAPS-1D simulation home window

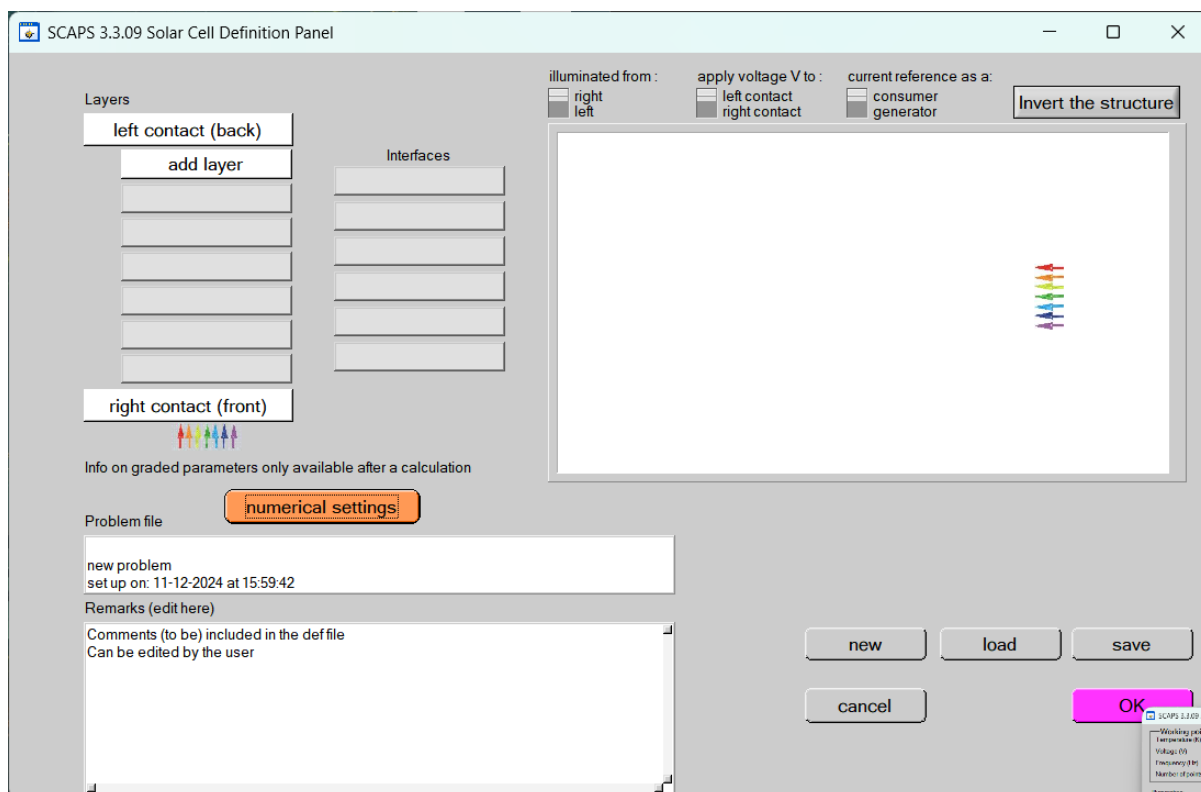


Figure 2.3: SCAPS-1D simulation working window showing layers

# **CHAPTER 3**

## **METHODOLOGY**

### **3.1 Material Selection and synthesis**

Argentum Zinc Fluoride ( $\text{AgZnF}_3$ ), is the compound being looked into for promising performance in photovoltaic applications. It possesses qualities needed for solar energy conversion, imparting such as high thermal stability, light absorption capability, and charge transportability.

With a bandgap set at 1.52 eV, the compound is able to absorb more than enough sunlight from across-the-solar-spectrum band. Good photon utilization means lesser energy to conversion efficiency. Unlike conventional lead-based perovskites,  $\text{AgZnF}_3$  is non-toxic and hence environmentally safer.

The term argentum derives from the Latin word for silver (Ag), which is one of the main components of the compound.  $\text{AgZnF}_3$  is made up of silver (Ag), zinc (Zn), and fluorine (F) bonded ionically; this system leads to very different ionic, optical, and power behavior. When combined with optimized ETLs (Electron Transport Layers) and HTLs (Hole Transport Layers),  $\text{AgZnF}_3$  can achieve enhanced power conversion efficiency (PCE).

Theoretical calculations and data from existing literature [21] have been employed to explore its behavior and performance, contributing to the growing understanding of this compound's potential in material science.

**Composition:** The compound contains silver (Ag), zinc (Zn), and fluorine (F), and is found in the form of ionic bonds.

By combining silver (Ag), zinc (Zn), and fluoride (F), this compound exhibits fascinating ionic, electronic, and optical behaviours that position it as a promising candidate for use in optical devices, ion-exchange materials, and semiconducting technologies.

### **Why $\text{AgZnF}_3$ ?**

$\text{AgZnF}_3$  has a bandgap in the range of approximately 1.1 to 1.5 eV which is ideal for efficient light absorption in solar cell applications. The optical nature of this structure favors the absorption of photons, meaning solar absorber materials need to have this feature. Additionally,  $\text{AgZnF}_3$  is quite stable under harsh conditions such as intense sunlight and moist ambience. This stability is largely attributed to its covalent bonding that is strong enough, however, with a weak ionic character, making it a promising and lasting candidate for solar cell devices.

### **PROBLEMS USING $\text{AgZnF}_3$**

**AgZnF<sub>3</sub>** isn't one of the most commonly known materials in everyday applications, it could be a specific compound used in scientific or industrial contexts. AgZnF<sub>3</sub> contains silver (Ag), zinc (Zn), and fluorine (F). Thus, the production of **AgZnF<sub>3</sub>** might require specific conditions or costly reagents. Silver (Ag), is a relatively expensive metal, and the synthesis of a compound involving both silver and zinc with fluorine could involve complex processes or high costs. This makes it less economical for large-scale consumer use.

**But** in comparison to that it gives efficiency >30% which is so much for any kind of solar cell. Also, in terms of toxicity it is non-toxic compared to lead based perovskites in the environment.

AgZnF<sub>3</sub> is chemically feasible material [18, 19, 20]

## Cost of the Materials

For the synthesis of AgZnF<sub>3</sub>, the raw materials are Silver (Ag), which is available at Rs 94600 per kilogram and Zinc which is available at Rs. 270 per kg and the Fluorine (F) is supplied as fluorine gas with a cost of Rs. 2500 per kg. Thus, we can say that the perovskite AgZnF<sub>3</sub> is costly. But it is quite good in output.

## SYNTHESIS of AgZnF<sub>3</sub>

- **Sol-gel Process** - metal alkoxides or salts are used as precursors, and the synthesis occurs in a gel form, followed by heat treatment to form the fluoride compound.
- **Solid state reaction** -  
$$\text{AgNO}_3 (\text{aq}) + \text{ZnCl}_2 (\text{aq}) + 3\text{NH}_4\text{F} (\text{aq}) \rightarrow \text{AgZnF}_3 (\text{s}) + 2\text{NH}_4\text{Cl} (\text{aq})$$
- **Hydrothermal or solvothermal synthesis** - synthesis of AgZnF<sub>3</sub> in a high-pressure vessel (autoclave) under controlled temperature and solvent conditions

**Characterization:** AgZnF<sub>3</sub> material can be characterized via X-ray diffraction (XRD) for crystal structure, scanning electron microscopy (SEM) for morphology, energy-dispersive X-ray spectroscopy (EDX) for elemental analysis.

## 3.2 SCAPS Simulation Setup

SCAPS (Solar Cell Capacitance Simulator) is a powerful simulation tool used to model the electrical characteristics of solar cells. It allows the simulation of current-voltage (I-V) characteristics, capacitance-voltage (C-V) curves, and quantum efficiency for different types of solar cells, including silicon, perovskite, and organic solar cells. For the simulations we employed the 1D Solar Cell Capacitance Simulator (SCAPS-1D) software, version 3.3.09. For modelling the perovskite PSC's, SCAPS-1D simulation code, designed by the ELIS department at gent university, was employed. Using the PV SCAPS-1D software a broad

variety of device frameworks can be investigated and designed with the help of accurate and realistic back-end physical equations [20,22]. SCAPS-1D software is a computational tool designed to simulate key photovoltaic processes in solar cells, like particular light absorption, charge carrier generation, transport and collection of charge carriers, and recombination losses. This software enables the modelling of solar cell and enables detailed evaluation of a solar cell's performance characteristics. The relation between charge density and electrostatic potential is defined by the Poisson's equation as Equation (3.1). The foundation for understanding how electric fields and charge distributions interact in the semiconductor layers, critical for optimizing efficiency and minimizing losses can be understood by using the Poisson's equation[20,23,24]. The electron and hole continuity equations are used to ascertain the characteristics related to a solar cell's quality. Additionally, Shockley-Read-Hall (SRH) recombination statics are incorporated into the program to model how the device operates.

$$\frac{d^2}{dx^2} \psi(x) = \frac{q}{\epsilon_0 \epsilon_r} [p(x) - n(x) + N_D - N_A + \rho_p - \rho_n] \quad (3.1)$$

In this equation,  $\psi$  represents the electrostatic potential. The equation incorporates material specific properties such as  $\epsilon_r$  (dielectric constant of the material or relative permittivity) and  $\epsilon_0$  (permittivity of vacuum, a fundamental constant).  $N_D$  and  $N_A$  denoting the donor dopant density and the acceptor dopant density. Also, the  $\rho_p$  represents the hole charge density while  $\rho_n$  represents the electrons charge density respectively. The terms  $n$  and  $p$  represent the holes and electrons concentrations correspondingly.

$$\frac{\delta p}{\delta t} = \frac{1}{q} \frac{\delta J_p}{\delta x} + (G_p - R_p) \quad (3.2)$$

$$\frac{\delta n}{\delta t} = \frac{1}{q} \frac{\delta J_n}{\delta x} + (G_n - R_n) \quad (3.3)$$

In the context of the Equation (3.2) and Equation (3.3),  $J_p$  denote the current densities of holes and  $J_n$  denotes the electrons. The terms  $G_p$  and  $R_p$  represents the hole generation and recombination rates, while  $G_n$  and  $R_n$  represents generation and recombination rates of electrons.

SCAPS-1D software resolves these behaviours by numerically solving two fundamental equations, equation of continuity and the Poisson's equation at material interfaces and electrical contacts for the charge carriers. SCAPS-1D software computes the steady-state response in 1D by considering the given equations and applying the boundary conditions.

The formula for the following results used in SCAPS are in the Equations (3.4, 3.5, 3.6 and 3.7)

$$PCE = \frac{V_m \cdot J_m}{P_{in}} \times 100 \quad (3.4)$$

$$FF = \frac{J_{mp} \times V_{mp}}{J_{sc} \times V_{oc}} \quad (3.5)$$

$$V_{oc} = \frac{k_B T}{q} \ln \left( \frac{J_{sc}}{J_0} + 1 \right) \quad (3.6)$$

$$J_{sc} = q \cdot \Phi_{in} \cdot \eta_{abs} \cdot \eta_{col} \quad (3.7)$$

Where,

$V_m$  and  $J_m$  are the voltage and current at maximum power point.

$V_{oc}$  is the open-circuit voltage

$J_{sc}$  is the short-circuit current

$J_0$  is the saturation current

$P_{in}$  is the incident power

$\Phi_{in}$  is the incident light flux

$\eta_{abs}$  is the absorption efficiency.

$\eta_{col}$  is the collection efficiency

To use SCAPS

- First, we open the SCAPS 1D software on our laptop
- Click on the Set Problem Now we define the Layer Structure such as ETL, HTL, absorber layer
- Define material Properties such as bandgap, electron affinity, mobility, dielectric constant, density of states, donor densities.
- Define the electrical contacts.
- We modify our software according to the properties of the materials such as temperature, resistance, or light intensity.
- Run simulation and analyze results. By doing so we can get our results such as efficiency, fill factor, current-voltage characteristics and quantum efficiency curve.

## 3.3 Device Architecture

### 3.3.1 AgZnF<sub>3</sub>

The study employs numerical simulations to analyse perovskite solar cells based on the AgZnF<sub>3</sub> absorber layer. The incorporation of a 200 nm thick AgZnF<sub>3</sub> layer with a bandgap of 1.52 eV [18] significantly gives better performance of the perovskite based solar cells alongside appropriate substitutes to conventional HTL, ETL, and back

contact materials. To achieve optimal performance, the solar cell is structured as (FTO/ETL/AgZnF<sub>3</sub>/HTL/Au) with AgZnF<sub>3</sub> serves as absorber layer. In this configuration, the fluorine doped tin oxide (FTO) layer functions as a transparent conductive oxide, allowing the light to pass through while efficiently collecting and transporting the charges, while gold (Au) serves as back anode contact, collecting holes and ensuring efficient charge extraction. The perovskite solar cells are designed in the n-i-p planer configuration, where the layers are sequentially stacked to form the device. The n-region represents electron transport layer (ETL), functions as electron selective contact. The intrinsic i region is the perovskite absorber layer, which serves as light harvesting core. And p-region denotes hole transport layer (HTL). When the cell is exposed to light, the perovskite intrinsic i layer produces excitons, which are coulombic pairs composed of a hole and an electron. The exciton produced dissociate at the boundaries between the ETL/absorber and HTL/absorber due to build-in electric fields. Electrons are extracted via the ETL, while the hole migrates through the HTL, minimizing recombination losses. The Electric field that exists at the interfaces between these layers accelerates exciton dissociation. Figure 2 presents a systematic evaluation of perovskite solar cell architecture using numerical SCAPS-1D simulations, comparing six ETLs and eight HTLs to determine the most efficient pairing. Figure illustrates band gap alignment of the perovskite Solar Cell. The various input parameters of different HTLs, ETLs, fluoride-based tin oxide and absorber layer are provided in **Error! Reference source not found.** and **Error! Reference source not found.**. The selection of potential ETLs and the HTLs for the perovskite solar cells, as shown in **Error! Reference source not found.** and **Error! Reference source not found.**, prioritizes material with high mobility of charge carrier and optimal electron affinity to improve charge transport and reduce energy losses. These characteristics directly counteract the  $V_{OC}$  deficit caused by nonradiative recombination that induces quasi-Fermi level splitting by decoupling electron and hole population under illumination. The band gap of the ETL plays a pivotal role in boosting the photogenerated carrier rate and prevents saturation of  $J_{SC}$  as perovskite absorber layer's thickness increases. The optimization of perovskite solar cells hinges on harmonizing the thickness of absorber and ETL to maximize light absorption while preserving the efficient charge extraction. The performance of the solar cells is governed by the interplay of multiple interdependent factors, each critically shaping efficiency and stability. These factors are ETL/HTL layers, thickness of absorber, series and shunt resistance and temperature. Our main goal of this research is to identify charge transport materials (ETLs/HTLs) that balance the optical and electrical properties to enhance the performance of solar cell. The simulations were conducted at an ambient temperature of 300 k with 100 mW/cm<sup>2</sup> of an incident power density and 1 MHz of frequency, under the Am 1.5G solar spectrum.

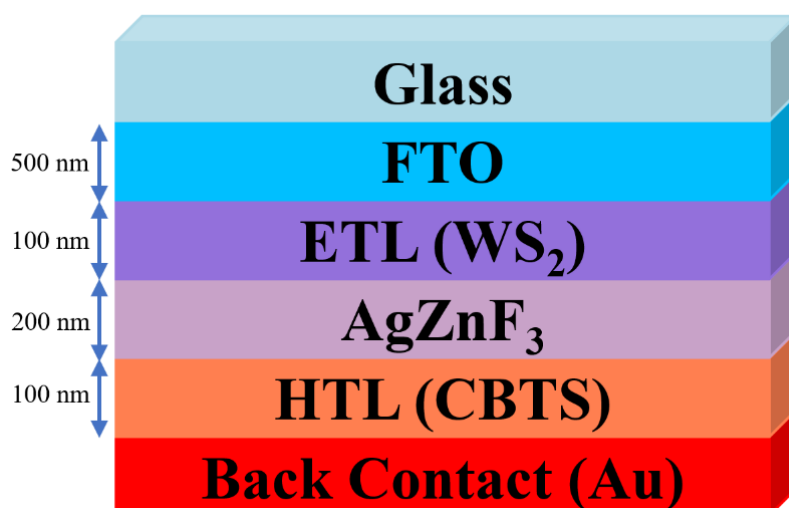


**Figure 2.1:** Device Architecture of AgZnF<sub>3</sub>-Based PSC.

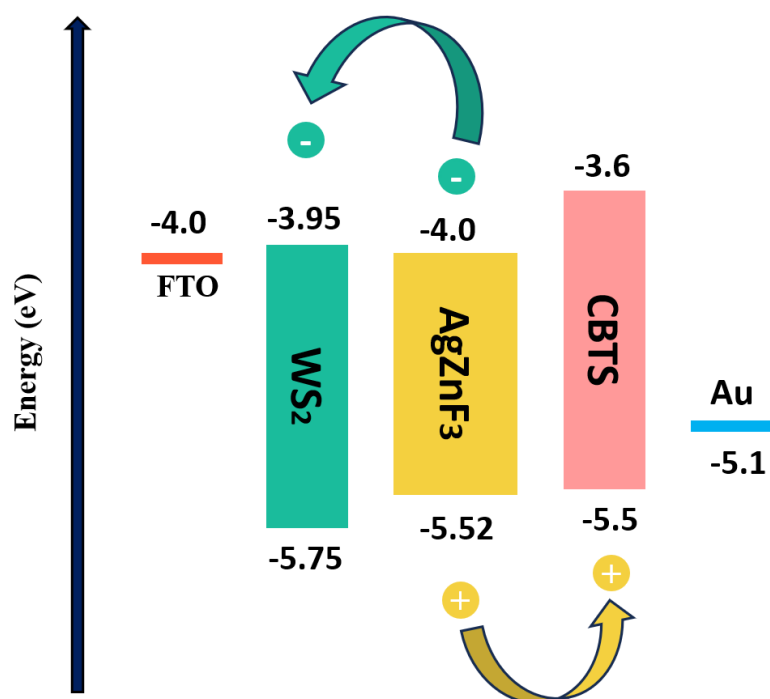


**Figure 3.2:** Band gap alignment of AgZnF<sub>3</sub>-based PSC.



### 3.3.2 HTLs and ETLs

ETL and HTL represent the electron transport layer and hole transport layer respectively

**Table 3.1** Simulation parameters of various ETLs.

Parameters	FTO [25–27]	TiO <sub>2</sub> [28,29]	PCBM [22,27]	C <sub>60</sub> [20,22]	WS <sub>2</sub> [20,22]	ZnSe [22]	CdS [30]	AgZnF <sub>3</sub> [19]
Thickness ( $\mu\text{m}$ )	0.500	0.100	0.100	0.100	0.100	0.100	0.100	0.200
E <sub>g</sub> (eV)	3.5	3.2	2	1.7	1.8	2.81	2.42	1.52
$\chi$ (eV)	4	4	3.9	3.9	3.95	4.09	4.4	4.0
$\epsilon_r$	9	9	3.9	4.2	13.6	8.6	10	2.9
N <sub>C</sub> (cm <sup>-3</sup> )	$2.2 \times 10^{18}$	$2 \times 10^{18}$	$2.5 \times 10^{21}$	$8 \times 10^{19}$	$1 \times 10^{18}$	$2.2 \times 10^{18}$	$2.2 \times 10^{18}$	$7.579 \times 10^{18}$
N <sub>V</sub> (cm <sup>-3</sup> )	$1.8 \times 10^{19}$	$1.8 \times 10^{19}$	$2.5 \times 10^{21}$	$8 \times 10^{19}$	$2.4 \times 10^{19}$	$1.8 \times 10^{18}$	$1.8 \times 10^{19}$	$4.026 \times 10^{19}$
V <sub>e</sub> (cm/s)	$1 \times 10^7$	$1 \times 10^7$	$1 \times 10^7$	$1 \times 10^7$	$1 \times 10^7$	$1 \times 10^7$	$1 \times 10^7$	$1 \times 10^7$
V <sub>h</sub> (cm/s)	$1 \times 10^7$	$1 \times 10^7$	$1 \times 10^7$	$1 \times 10^7$	$1 \times 10^7$	$1 \times 10^7$	$1 \times 10^7$	$1 \times 10^7$
$\mu_n$ (cm <sup>2</sup> /Vs)	20	20	0.2	$8 \times 10^{-2}$	100	400	100	695
$\mu_h$ (cm <sup>2</sup> /Vs)	10	10	0.2	$3.5 \times 10^{-3}$	100	110	25	27
N <sub>A</sub> (cm <sup>-3</sup> )	0	0	0	0	0	0	0	$6.260 \times 10^{20}$
N <sub>D</sub> (cm <sup>-3</sup> )	$1 \times 10^{19}$	$9 \times 10^{16}$	$2.93 \times 10^{17}$	$1 \times 10^{17}$	$1 \times 10^{18}$	$1 \times 10^{15}$	$1 \times 10^{15}$	0
N <sub>t</sub> (cm <sup>-3</sup> )	$1 \times 10^{14}$	$1 \times 10^{14}$	$1 \times 10^{14}$	$1 \times 10^{14}$	$1 \times 10^{14}$	$1 \times 10^{14}$	$1 \times 10^{14}$	$1 \times 10^{14}$

**Table 3.2** Simulation parameters of various HTLs

Parameters	Zn <sub>2</sub> P <sub>3</sub> [31]	CBTS [22,28]	P <sub>3</sub> HT [22]	MASnBr <sub>3</sub> [28]	Spiro- OMeTAD [28]	CuO [22]	MOS <sub>2</sub> [30]	PEDOT: PSS [22]
Thickness ( $\mu\text{m}$ )	0.250	0.100	0.050	0.200	0.200	0.050	0.050	0.050
E <sub>g</sub> (eV)	1.5	1.9	1.7	2.15	3.0	1.51	1.7	1.6
$\chi$ (eV)	4.2	3.6	3.5	3.39	2.2	4.07	3.8	3.4
$\epsilon_r$	7.11	5.4	3	8.2	3	18.1	13.60	3
N <sub>C</sub> (cm <sup>-3</sup> )	$2.2 \times 10^{18}$	$2.2 \times 10^{18}$	$2 \times 10^{21}$	$1 \times 10^{20}$	$2.2 \times 10^{18}$	$2.2 \times 10^{19}$	$2.8 \times 10^{19}$	$2.2 \times 10^{18}$
N <sub>V</sub> (cm <sup>-3</sup> )	$1.8 \times 10^{19}$	$1.8 \times 10^{19}$	$2 \times 10^{21}$	$1 \times 10^{18}$	$1.8 \times 10^{19}$	$5.5 \times 10^{20}$	$1 \times 10^{19}$	$1.8 \times 10^{19}$
V <sub>e</sub> (cm/s)	$1 \times 10^7$	$1 \times 10^7$	$1 \times 10^7$	$1 \times 10^7$	$1 \times 10^7$	$1 \times 10^7$	$1 \times 10^7$	$1 \times 10^7$
V <sub>h</sub> (cm/s)	$1 \times 10^7$	$1 \times 10^7$	$1 \times 10^7$	$1 \times 10^7$	$1 \times 10^7$	$1 \times 10^7$	$1 \times 10^7$	$1 \times 10^7$
$\mu_n$ (cm <sup>2</sup> /Vs)	1	30	$1.8 \times 10^{-3}$	1.6	$2.1 \times 10^{-3}$	100	12	$4.5 \times 10^{-2}$
$\mu_h$ (cm <sup>2</sup> /Vs)	3.8	10	$1.86 \times 10^{-2}$	1.6	$2.16 \times 10^{-3}$	0.1	2.8	$4.5 \times 10^{-2}$
N <sub>A</sub> (cm <sup>-3</sup> )	$1 \times 10^{19}$	$1 \times 10^{18}$	$1 \times 10^{18}$	$1 \times 10^{18}$	$1 \times 10^{18}$	$1 \times 10^{18}$	$1 \times 10^{19}$	$1 \times 10^{18}$
N <sub>D</sub> (cm <sup>-3</sup> )	0	0	0	0	0	0	0	0
N <sub>t</sub> (cm <sup>-3</sup> )	$1 \times 10^{14}$	$1 \times 10^{14}$	$1 \times 10^{14}$	$1 \times 10^{14}$	$1 \times 10^{14}$	$1 \times 10^{14}$	$1 \times 10^{14}$	$1 \times 10^{14}$

# CHAPTER 4

## RESULTS AND DISCUSSION

### 4.1 Calculation of different AgZnF<sub>3</sub> parameters for simulation

The simulation parameters of the AgZnF<sub>3</sub> perovskite layer such as band gap, dielectric relative permittivity, electron/hole mobility and uniform shallow donor density and acceptor density were adopted from prior experimental and computational studies on AgZnF<sub>3</sub>. But, conduction band density of states ( $N_A$ ) and density of states of valence band ( $N_V$ ) are determined using the established theoretical Equation (4.1) and (4.2). [28,32,33]

$$N_C = 2 \left( \frac{2\pi k_B T m_e^*}{h^2} \right)^{3/2} \quad (4.1)$$

$$N_V = 2 \left( \frac{2\pi k_B T m_h^*}{h^2} \right)^{3/2} \quad (4.2)$$

In these equations, the  $m_e^*$  and  $m_h^*$  denotes the effective mass of the electrons and effective mass of holes respectively, which vary depending on the material properties. For AgZnF<sub>3</sub>, the density of states effective masses ( $m_{dos}$ ) for electrons and holes is 0.45 and 1.37 respectively[19]. The Conduction band DOS ( $N_C$ ) and valence band DOS ( $N_V$ ) are computed to be  $7.579 \times 10^{18} \text{ cm}^{-3}$  and  $4.026 \times 10^{19} \text{ cm}^{-3}$  by using Equation (4.1) and Equation (4.2).

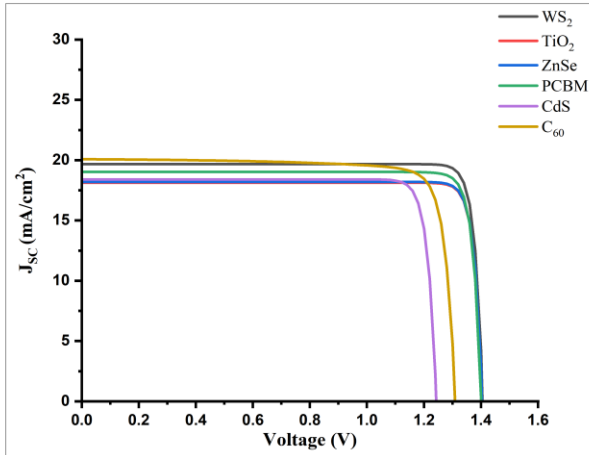


**Figure 4.1:** J-V Characteristics of different ETLs with CBTS as HTL.

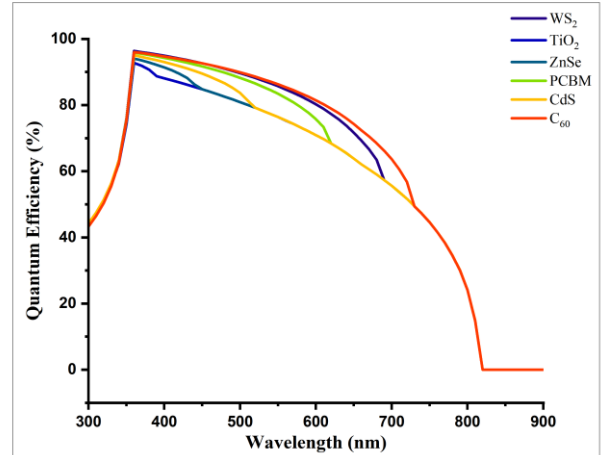


**Figure 4.2:** QE curves of different ETLs with CBTS as HTL.

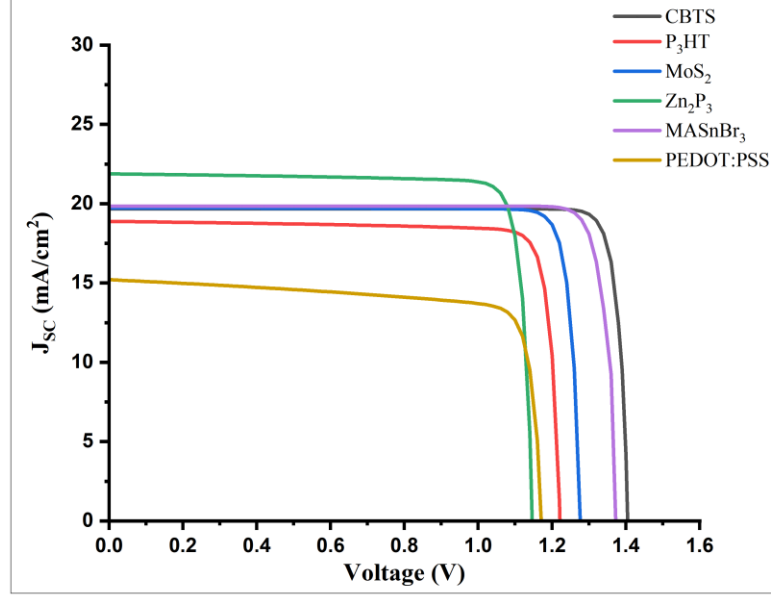


**Figure 4.3:** J-V characteristics of different HTLs with WS<sub>2</sub> as ETL.

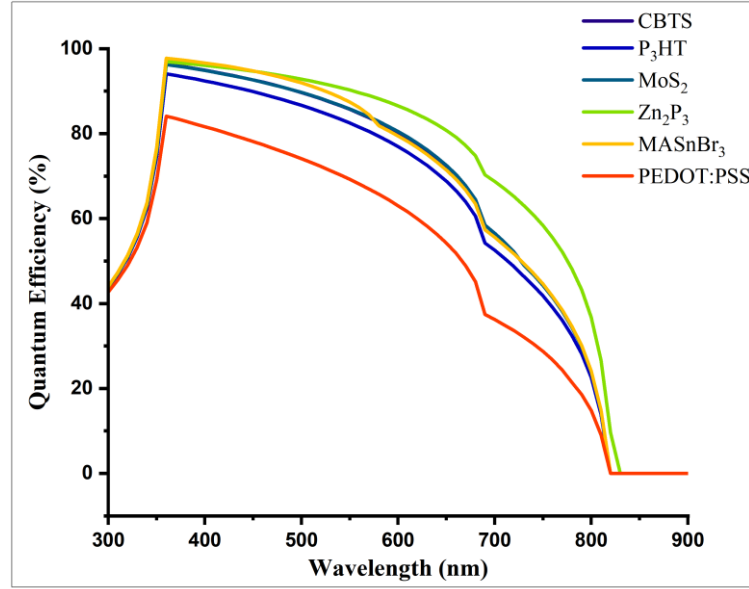


**Figure 4.4:** QE plots of different HTLs with WS<sub>2</sub> as ETL.

The AgZnF<sub>3</sub> perovskite material exhibits a  $E_g$  of 1.52 eV. With, the holes mobility ( $\mu_h$ ) of the material is  $27 \text{ cm}^2 \text{ V}^{-1} \text{ s}^{-1}$  and the electrons mobility ( $\mu_n$ ) of the material is  $695 \text{ cm}^2 \text{ V}^{-1} \text{ s}^{-1}$  [19]. The electrons and holes possess a thermal velocity of  $1 \times 10^7 \text{ cm s}^{-1}$ , indicating their movement due to thermal agitation within the material. The defect density for the material is chosen to  $1 \times 10^{14} \text{ cm}^{-3}$  initially. The dielectric permittivity (relative) of the material is 2.90 [34]. For simulations, the electron affinity was initially assumed to be 4.0 eV, followed by systematic optimization to determine its ideal value. AgZnF<sub>3</sub> exhibits a non-degenerate p-type conductivity characterized by a uniform shallow acceptor density ( $N_A$ ) =  $6.260 \times 10^{20} \text{ cm}^{-3}$  with no donor contribution ( $N_D = 0$ ), resulting in hole carriers as the majority under thermal equilibrium[19].

## 4.2 Exploring ETLs Variations

ETL stands for the electron transfer layer which plays a critical role on solar cells by efficiently transporting the electrons from perovskite active layer to the electrode and simultaneously blocking the holes to reduce the recombination loss. It facilitates the extraction of light-generated electrons from the perovskite layer and directing their movement towards the cathode which is the back contact metal Au. By ensuring efficient electron transfer, the ETL helps to prevent charge combination and thereby optimizing electrical current generation and enhances the device's overall performance and power conversion efficiency. We have assessed the structure FTO/ETL/AgZnF<sub>3</sub>/CBTS/Au by varying six ETLs with serving CBTS as HTL with Au as the back contact metal. We have taken thickness of the absorber layer-AgZnF<sub>3</sub> as 200 nm during simulations, with  $N_t$  of  $10^{14} \text{ cm}^{-3}$ . The chosen ETLs were prioritized based on their better performance outcomes and their superior performance in prior research, where they demonstrated significant enhancement in photovoltaic conversion efficiency. We have assessed the effects of distinct ETLs with respective thickness in the parentheses (TiO<sub>2</sub> (100 nm), PCBM (100 nm), C<sub>60</sub> (100 nm), WS<sub>2</sub> (100 nm), ZnSe (100 nm), CdS (100 nm)) on PSC performance using the FTO/ETL/AgZnF<sub>3</sub>/ABTS/Au architecture. The hole transport layer, CBTS, thickness was maintained at 100 nm and with defect concentration of  $10^{14} \text{ cm}^{-3}$ , the absorber layer was simulated. Simulations were conducted using SCAPS software and key parameters were analysed which includes Q.E. vs wavelength curves and J-V characteristics. The results were analysed and visualized using origin pro software. The J-V properties of the perovskite solar cell with CBTS as the HTL and varying electron transport layers are shown in Figure 3.1. Q.E., which evaluates the proportion of photogenerated charge carriers relative to the total incident photons, directly reflects the device efficiency to convert light into electrical energy. Q.E. vs wavelength plots for different ETL are presented in Figure 4.2 Q.E. initially increases with increasing wavelength, attaining a peak efficiency and then starts gradually

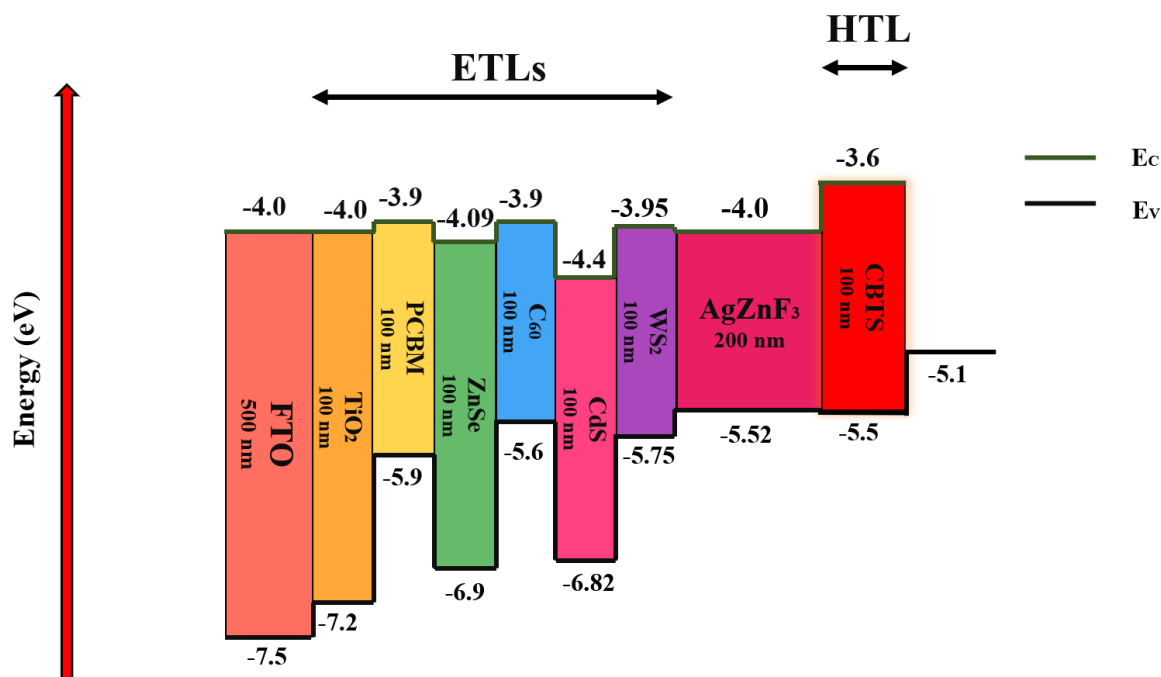
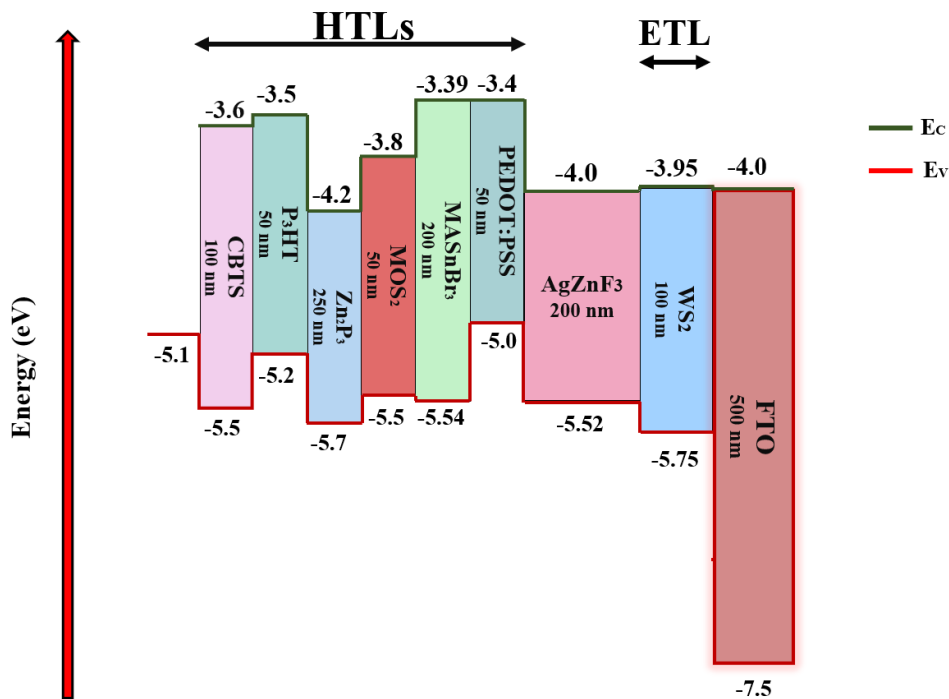


Figure 4.5: Band Diagram Analysis for FTO/ETLs/AgZnF<sub>3</sub>/CBTS/Au.

declining. The wavelength where the absorption decreases and Q.E. drops is referred as the cut-off wavelength. The decrease in Q.E. arises because of the enhanced charge recombination near the device's surface and lower absorption of lower energy photons at longer wavelength. Figure 4.5 shows the structure of PSC with different ETLs. The study of these ETLs specifies the optimized ETL for the PSC architecture and WS<sub>2</sub> emerged as the optimized ETL, delivering maximum Power conversion efficiency of 25.14 % and FF of 90.90 %. The input parameters for various ETLs are detailed in [Error! Reference source not found.](#). The PSC structure of FTO/WS<sub>2</sub>/AgZnF<sub>3</sub>/CBTS/Au gave PCE of 25.14 %. This performance surpasses the five other ETLs tested, owing to WS<sub>2</sub>'s better electronic properties, optimal optical characteristics, favourable energy level alignment and a wider bandgap **Fig**

### 4.3 Exploring HTLs Variations



**Figure 4.6:** Band Diagram Analysis for FTO/WS<sub>2</sub>/AgZnF<sub>3</sub>/HTLs/Au.

Hole transport layer (HTL) is an important component in the PSCs, responsible for selectively extracting and facilitating the movement of holes, which are positive charge carriers, from the active layer to anode. The efficient transfer of the holes is essential to prevent the charge combination, enabling the completion of electrical circuit. Optimized hole transport enhances charge collection but also improves the device's overall power conversion efficiency. We have assessed the solar cell architecture FTO/WS<sub>2</sub>/AgZnF<sub>3</sub>/HTL/Au by varying 8 HTLs with WS<sub>2</sub> serving as the electron transport layer and Gold (Au) as the back electrode. We have taken the thickness of the absorber layer-AgZnF<sub>3</sub> as 200 nm during simulations, with a  $N_t$  of  $10^{14} \text{ cm}^{-3}$ . The impact of 8 HTLs with respective thicknesses in the parentheses (P<sub>3</sub>HT (50 nm), CBTS (100 nm), Zn<sub>2</sub>P<sub>3</sub> (250 nm), MASnBr<sub>3</sub> (200 nm), Spiro-OMeTAD (200 nm), MOS<sub>2</sub> (50 nm), CuO (50 nm), PEDOT: PSS (50 nm)) is investigated. The electron transport layer (WS<sub>2</sub>) was fixed at 100 nm thickness, and the absorber layer (AgZnF<sub>3</sub>) was simulated with  $N_t$  of  $10^{14} \text{ cm}^{-3}$  and a thickness of 200 nm. Using the SCAPS-1D software, we analysed key parameters, including

current-voltage behaviour and quantum efficiency as a function of wavelength, and visualized the results using origin pro software. J-V curves of different HTLs with WS<sub>2</sub> as ETL are shown in Figure 4.3. Quantum efficiency variation with the absorbed wavelength for different HTLs is shown in Figure 4.4. The observed decrease in Q.E. is because of the increased surface recombination, which reduces charge carrier collection, and lower photon absorption at longer wavelength. The point where quantum efficiency drops is defined as the cut-off wavelength. Different HTLs band alignment with the SC structure is shown in **Fig** This study identifies, the optimized HTL for the FTO/WS<sub>2</sub>/AgZnF<sub>3</sub>/HTL/Au architecture. This comparison aims to identify the HTL configuration that optimizes hole transport, minimizes recombination and to maximize the device's power conversion efficiency. CBTS (band gap = 1.9 eV)

CBTS gives better power conversion efficiency – 25.14% with a FF (fill factor) of 90.90%. among the 8 HTLs used. CBTS superior performance stems from its wider bandgap, which enhances the alignment of energy levels between perovskite absorber and the electron transport layer Figure 4.6.

**Table** provides the comparative analysis of different photovoltaic characteristics for various AgZnF<sub>3</sub>-based perovskite solar cell configurations with different HTLs and ETLs.

**Table 4.1** Comparative analysis of Photovoltaic (PV) Parameters of AgZnF<sub>3</sub> based PSC.

Device Structure	V <sub>oc</sub> (V)	J <sub>sc</sub> (mA/cm <sup>2</sup> )	FF %	PCE%
FTO/WS <sub>2</sub> /AgZnF <sub>3</sub> /P <sub>3</sub> HT/Au	1.22	18.88	87.40	20.16
FTO/WS <sub>2</sub> /AgZnF <sub>3</sub> /CBTS/Au	1.40	19.67	90.90	25.14
FTO/WS <sub>2</sub> /AgZnF <sub>3</sub> /MoS <sub>2</sub> /Au	1.27	19.73	89.90	22.66
FTO/WS <sub>2</sub> /AgZnF <sub>3</sub> /Zn <sub>2</sub> P <sub>3</sub> /Au	1.14	21.87	87.47	21.96
FTO/WS <sub>2</sub> /AgZnF <sub>3</sub> /Spiro-OMeTAD/Au	1.34	19.55	90.38	23.77
FTO/WS <sub>2</sub> /AgZnF <sub>3</sub> /MASnBr <sub>3</sub> /Au	1.40	19.85	87.87	24.50
FTO/WS <sub>2</sub> /AgZnF <sub>3</sub> /CuO/Au	1.12	10.04	81.02	9.18
FTO/WS <sub>2</sub> /AgZnF <sub>3</sub> /PEDOT:PSS/Au	1.17	15.20	79.84	14.23
FTO/TiO <sub>2</sub> /AgZnF <sub>3</sub> /CBTS/Au	1.40	18.12	90.93	23.14
FTO/PCBM/AgZnF <sub>3</sub> /CBTS/Au	1.40	19.03	90.27	24.06
FTO/C <sub>60</sub> /AgZnF <sub>3</sub> /CBTS/Au	1.30	20.08	84.44	22.21
FTO/ZnSe/AgZnF <sub>3</sub> /CBTS/Au	1.40	18.19	90.93	23.22
FTO/CdS/AgZnF <sub>3</sub> /CBTS/Au	1.24	18.40	89.41	20.47

## 4.4 Thickness variation in Absorber Layer

Optimizing the thickness of the perovskite light-absorber layer is essential for achieving peak performance in PSCs. Light harvesting improvement and charge carrier transport, effective extraction of electrons and holes to minimize the recombination losses, are significantly governed by the absorber layer's thickness. To study the influence of absorber layer's thickness on key performance metrics, including power conversion efficiency, full factor and current density, we carried out batch calculations using SCAPS-1D software. In these simulations, the absorber layer thickness was adjusted in increments of 100 nm while its density was held steady at  $1 \times 10^{14} \text{ cm}^{-3}$  and the temperature was maintained at 300 K. All other parameters, including those of n-type transport layer ( $\text{WS}_2\text{-ETL}$ ), p-type transport layer ( $\text{CBTS-HTL}$ ), and FTO conductive layer remains unchanged. The thickness of the absorber layer was studied across a wide range, starting at 100 nm and extending up to 1000 nm, to assess its impact.

Simulations revealed that efficiency escalates with absorber thickness until 1000nm and after that there was no significant increase. Thicker absorber layer allows for better absorption of incident photons, resulting in higher electron and hole pairs and boosting photocurrent and improves device's efficiency. However, at high thickness ( $>1000 \text{ nm}$ ), perovskite solar cell efficiency rises minimally and then it begins to decrease. This is because of increase in recombination losses in the thicker absorber layer. We observed maximum efficiency of 33.40 % at thickness of 1000 nm and minimum efficiency of 19.84 % at 100 nm thickness. The  $J_{\text{SC}}$  rises to its maximum value of  $26.80 \text{ mA cm}^{-2}$  at

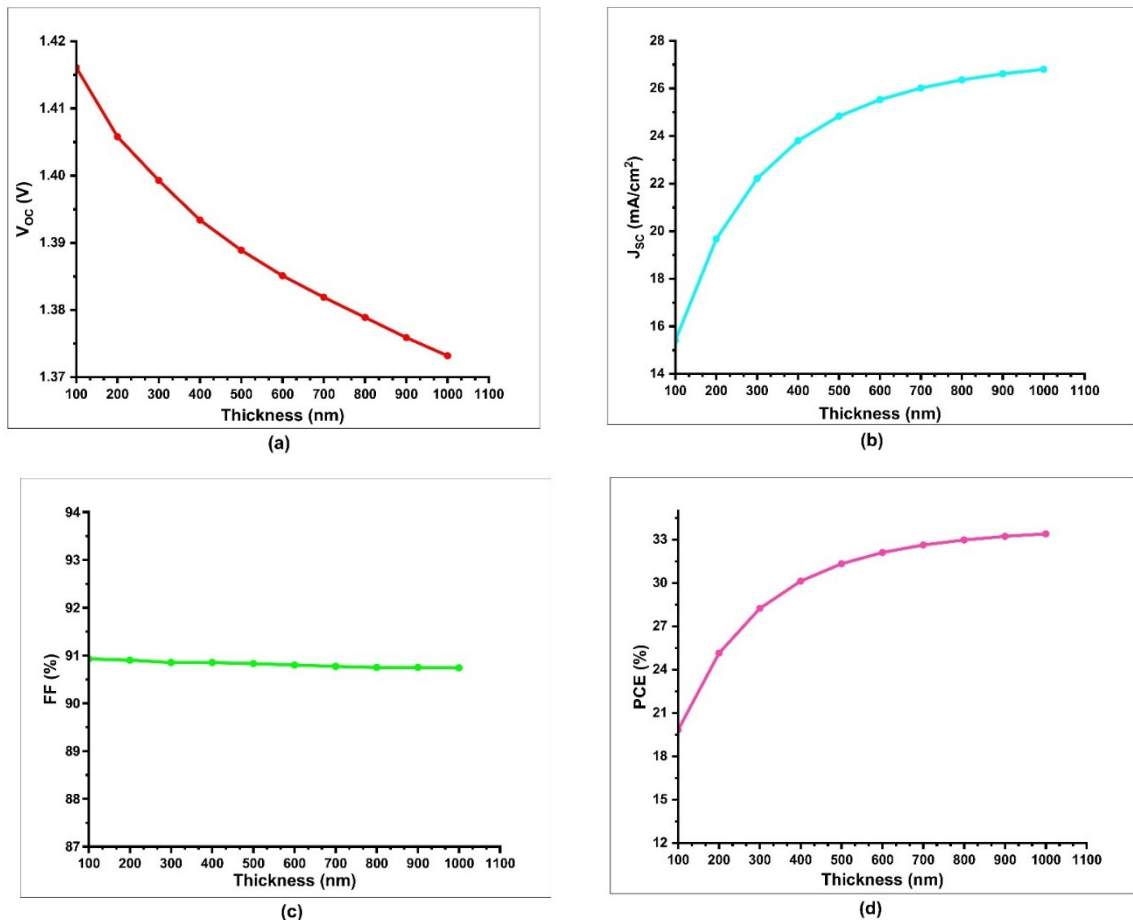


**Figure 4.7:** impact of variation in thickness on PV Parameters (a)  $V_{\text{oc}}$ , (b)  $J_{\text{sc}}$ , (c) FF, (d) PCE.

1000 nm. The value of Fill Factor is maximum for 100 nm thickness and decreased from 90.93 to 90.74 at 1000 nm thickness. Similar decrease is observed in value of open circuit current voltage as the thickness increases. The efficiency of perovskite solar cell exhibits minimal improvement after an absorber layer thickness of 550 nm, accompanied by decrease in fill factor and  $V_{OC}$ . This is because of increased series resistance at greater thickness and thus 550 nm thickness is identified as optimum thickness.

The active layer's thickness is crucial for optimizing the PCE of the solar cells. Appropriately chosen thickness maximizes photocurrent generation and thereby current density and minimizes reverse saturation current. However, as absorber layer becomes thicker, the reduced electric field negatively affects charge carrier recombination, thereby decreasing efficiency. Moreover, increased absorber thickness leads to reduction in FF due to increased series resistance and increased power loss within the device[28]. The increment in thickness leads to a rise in dark saturation current, which facilitates the charge carrier's recombination and hence the  $V_{OC}$  falls [28,35]. The change in FF,  $J_{SC}$ ,  $V_{OC}$ , and PCE with thickness is shown in Figure 4.7.

## 4.5 Optimization of absorber layer defect density

Minimizing the defect density ( $N_t$ ) in the perovskite light-absorber layer is essential for improving the performance of PV devices. High  $N_t$  amplifies the charge carrier's recombination, which impacts the performance. Defects in PSCs acts as recombination centres where electrons and holes pair up and recombine, leading to a reduction in photocurrent and decreases solar cell's overall efficiency.

To study the influence of  $N_t$  in the absorber layer-AgZnF<sub>3</sub>, Batch calculations were performed using SCAPS simulation software. Results showed that, below  $10^{10} \text{ cm}^{-3}$  the PCE and other associated parameters remained constant and after  $10^{10} \text{ cm}^{-3}$ ,  $N_t$  was varied in increments of order of  $10^1$  while maintaining a fixed absorber thickness value of 550 nm. All other parameters of the absorber layer, HTL, ETL and FTO were kept same as mentioned in **Error! Reference source not found.** and **Error! Reference source not found.** The  $N_t$  was varied across a wide range, beginning at  $10^{13} \text{ cm}^{-3}$  and extending to  $10^{18} \text{ cm}^{-3}$  to analyse the impact. An inverse relation between  $N_t$  and device efficiency was observed. At  $N_t$  of  $10^{13} \text{ cm}^{-3}$  the solar cell exhibited a high efficiency of 33.12%. As  $N_t$  rose the efficiency of the device decreases and becomes 13.92 % at  $N_t$  of  $10^{18} \text{ cm}^{-3}$ . The FF of the device drops down to 77.14 % at  $10^{18} \text{ cm}^{-3}$  which was 91.04 % at  $10^{13} \text{ cm}^{-3}$ . Similar drop was seen in  $V_{OC}$  and  $J_{SC}$  value. That due to fact that higher defect density increased carrier recombination rates, which increases, the dark saturation current ( $J_0$ ). This rise in  $J_0$  lowers the  $V_{OC}$  of the PSC. And lower  $V_{OC}$  reduces the potential difference that drives the current and leads to reduction of overall efficiency of the device. Fill factor reflects the cell's ability of how efficiently it converts the generated current into the usable power. And higher defect density increases the series resistance and internal power dissipation which in turn reduces FF. An optimum value of  $10^{14} \text{ cm}^{-3}$  was identified, balancing the recombination losses and performance and device achieves 31.76 % efficiency with FF of 90.82 % and  $V_{OC}$  of 1.38 V. High concentration of defects promotes charge recombination because of formation of pinholes, which results in faster



film degradation. This not only shortens the functional lifespan of the film but also weakens its structural integrity, ultimately resulting lower stability and decreases the overall performance[36].

Figure 4.8 illustrates the dependence of the key PV parameters -  $V_{OC}$ , FF, PCE and  $J_{SC}$  – on the  $N_t$  of the absorber layer.

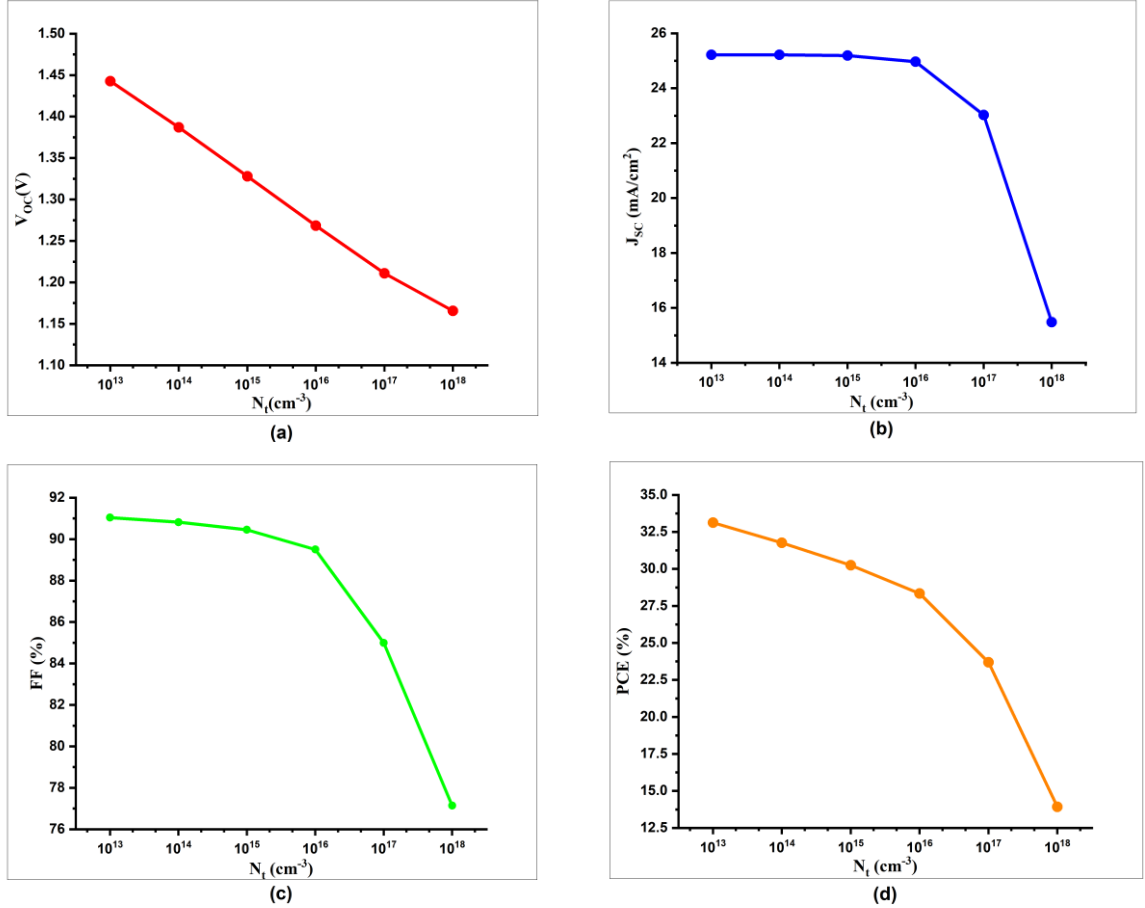


**Figure 4.8:** Impact of Variation in Defect Density on PV Parameters (a)  $V_{OC}$ , (b)  $J_{SC}$ , (c) FF, (d) PCE.

## 4.6 Impact of electron affinity

To optimize the electron affinity of the perovskite layer, the parameter was tuned across a wide range, starting at 3.4 eV and extending up to 4.6 eV while keeping fixed values for all other properties of absorber layer, ETL and HTL. The optimization is essential, as electron affinity plays a crucial role in defining the absorber layer's ability to facilitate efficient charge transport in photovoltaic devices. Electron affinity should be carefully tuned within the optimum range of alignment where both conduction band of absorber and ETL will match each other. The optimum electron affinity value for which efficiency of the cell is maximum is identified as 3.9 eV when thickness of the absorber is taken as 550 nm with defect concentration of  $1 \times 10^{14} \text{ cm}^{-3}$  simulated at 300 K temperature. The

PCE of the cell at  $\chi = 3.9$  reaches 31.77 %, featuring a high fill factor of 90.82 % and an open-circuit voltage of 1.38 V. Efficiency of SC increases with increase in the electron affinity up to 3.8 V, plateaus between 3.8 eV and 3.9 eV (with nearly same value of PCE in this range) and it then starts decreasing after 4.1 V. The value of PCE is nearly same for the 3.8 V and 3.9 V of the electron affinity.

Figure 4.9 illustrates the variations in key performance parameters –  $J_{SC}$ , PCE, FF and  $V_{OC}$  - as functions of  $N_t$ .

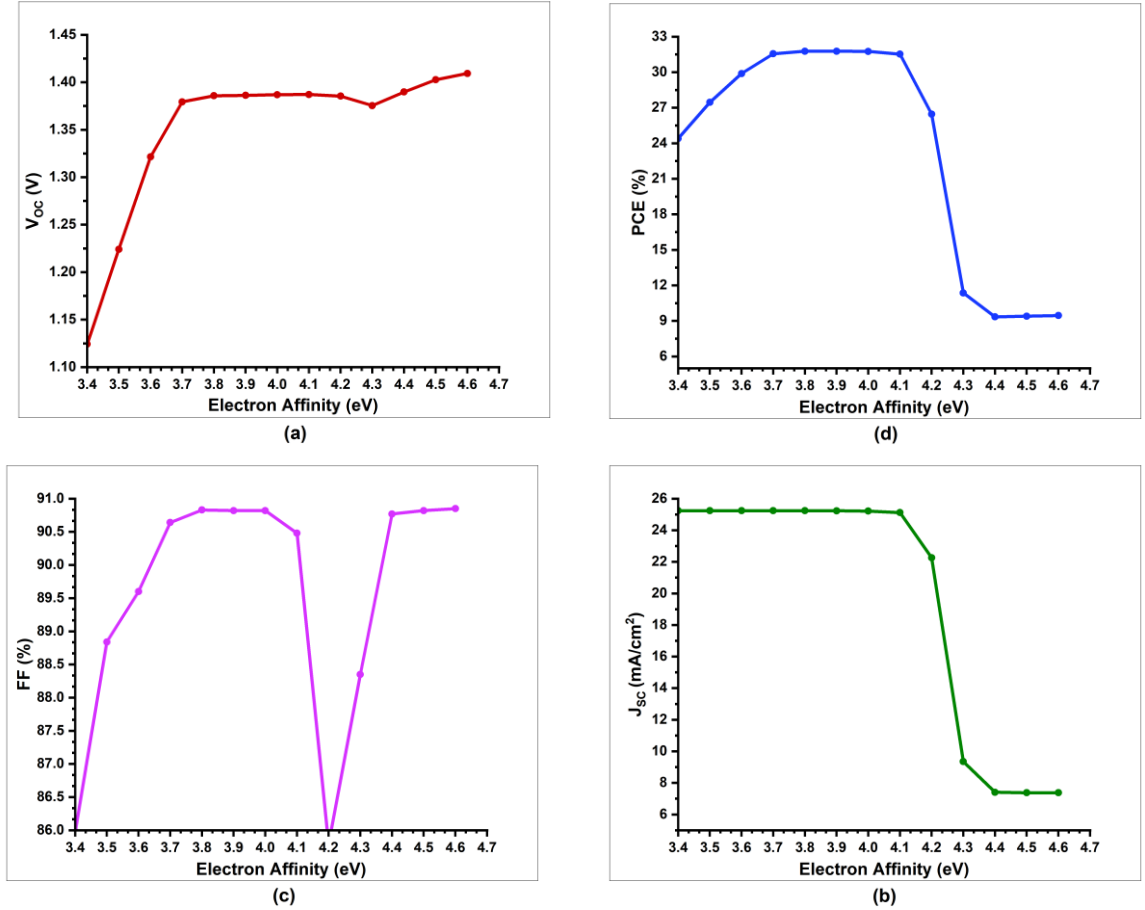


**Figure 4.9:** Impact of Variation in Electron Affinity on PV Parameters (a)  $V_{OC}$ , (b)  $J_{SC}$ , (c) FF, (d) PCE.

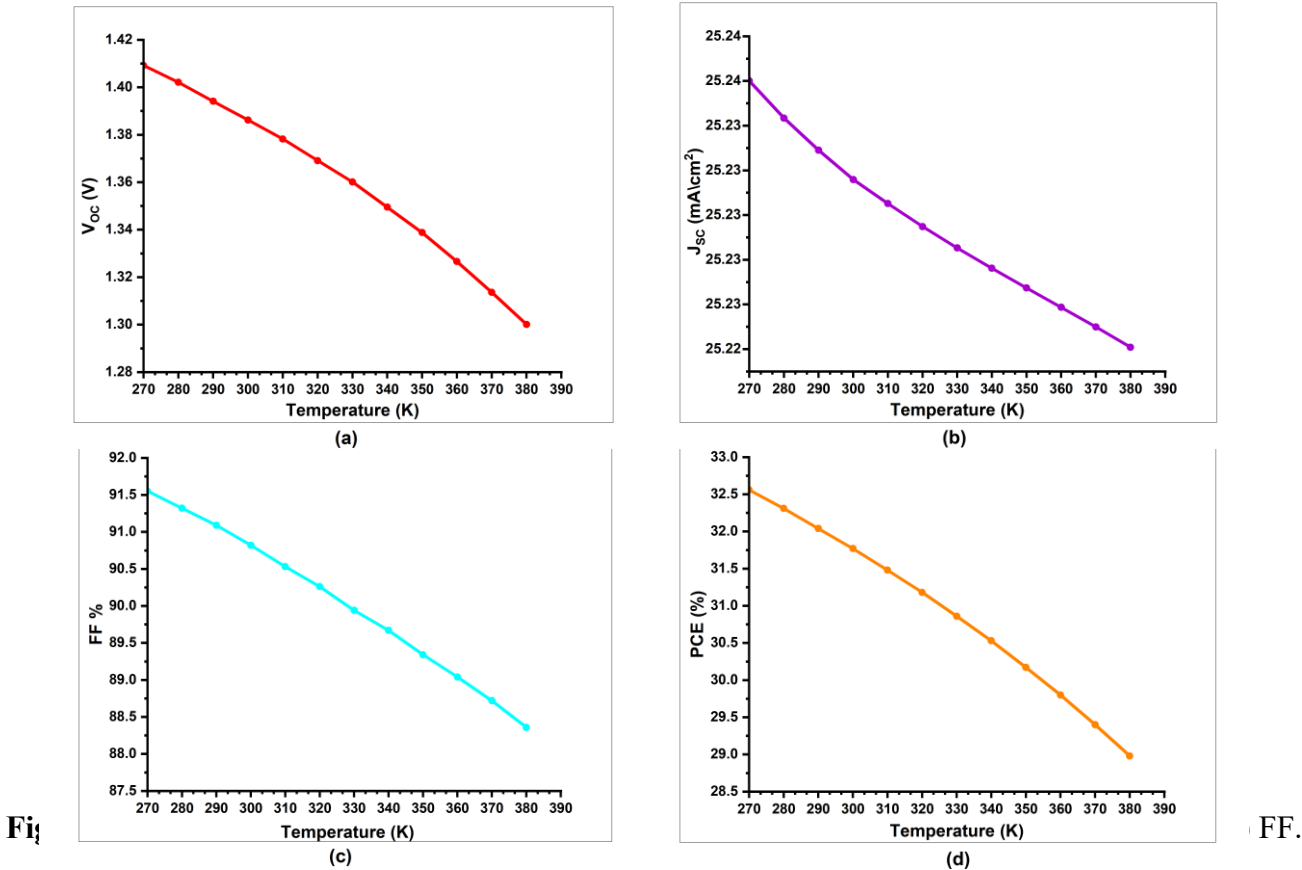
## 4.7 Effect of operating temperature

The performance of solar cells is significantly and critically impacted by temperature, making it a crucial factor in their overall efficiency. PSCs exhibit thermal instability when exposed to light and high temperatures [37]. Studies indicate that PSCs lose approximately 10% of their efficiency when operated for 1000 h at 85 °C, highlighting a substantially shorter lifespan compared to conventional silicon-based solar cells [38]. From the heat generated from the excessive solar radiation, the system's ability to efficiently extract charges is hindered. This thermal buildup results in energy loss, which degrades the device's operational efficiency and accelerates performance degradation.

over time. It is important to manage these temperature-linked effects to maintain good performance [39].

Figure 4.10 highlights the impact of the temperature changes, spanning from 270 K to 380 K on key performance metrics of solar cell, including fill factor (FF), open-circuit current voltage ( $V_{OC}$ ), short-circuit current density ( $J_{SC}$ ) and power conversion efficiency (PCE) under  $1000 \text{ Wm}^{-2}$  solar illumination. As the temperature rises, all the parameters exhibit a notable decline. At 270 K temperature, the efficiency of the device is 32.56% which is maximum with a maximum fill factor of 91.55%. However, these values progressively decrease with increasing temperature, highlighting the inverse relationship between operating temperature and overall cell performance. The solar panels are operated at temperature above 300 K and for that temperature the efficiency of the device exhibits reduced performance, with device efficiency 31.77% and a fill factor of 90.82%. When temperature rise further to 380 K, the efficiency of solar cell drops to 28.98% and fill factor decreases to 88.36%. Similar drops in the  $V_{OC}$  and  $J_{SC}$  were observed. This is because at higher temperature, thermal excitation of charge carriers takes place which increases intrinsic carrier concentration. Consequently, dark saturation current increases and dark current reduces the build-in potential across the device. This reduction in build-in potential directly lowers  $V_{OC}$ . Also, because of higher recombination rates and reduced carrier lifetime, density of available charge carriers decreases. This reduction raises series resistance and further hindering current extraction.

Figure 4.10 illustrates the temperature-dependent trends in solar cell’s key parameters –  $J_{SC}$ , PCE,  $V_{OC}$  and FF.



## 4.8 Effect of work function of back contact

The back metal electrode critically determines device efficiency and operational stability by modulating charge extraction efficiency, work function alignment, and interfacial interactions with the absorber layer. We varied five different back metal materials to ascertain the most efficacious one for the absorber layer. The five different metals with the work function in the parenthesis are gold, Au (5.10 eV), platinum, Pt (5.65 eV), nickel, Ni (5.04 eV), palladium, Pd (5.6 eV), Copper, Cu (4.94 eV).[40]

**Table 2.2** Performance Parameters of FTO/WS<sub>2</sub>/AgZnF<sub>3</sub>/CBTS Photovoltaic Devices with different Back Metals.

Device Structure	Metal Work function	V <sub>oc</sub> (V)	J <sub>sc</sub> (mA/cm <sup>2</sup> )	FF %	PCE%
FTO/WS <sub>2</sub> /AgZnF <sub>3</sub> /CBTS/Au	5.10 eV	1.38	25.23	90.82	31.77
FTO/WS <sub>2</sub> /AgZnF <sub>3</sub> /CBTS/Pt	5.65 eV	1.38	25.27	90.86	31.86
FTO/WS <sub>2</sub> /AgZnF <sub>3</sub> /CBTS/Pd	5.6 eV	1.38	25.27	90.86	31.86
FTO/WS <sub>2</sub> /AgZnF <sub>3</sub> /CBTS/Ni	5.04 eV	1.38	25.23	90.61	31.69
FTO/WS <sub>2</sub> /AgZnF <sub>3</sub> /CBTS/Cu	4.94 eV	1.37	25.23	87.90	30.50

Platinum (Pt, 5.65 eV) gives the maximum power conversion efficiency of 31.86% and 90.86% fill factor outperforming gold (Au, 5.10 eV) which achieves a slightly lower PCE of 31.77%. The performance parameters of photovoltaic device with different back metals with metal work functions are detailed in **Table 2.2**. This performance disparity of the five back metals is because of the work function alignment, electrical conductivity, and contact formation factors. Metals with high electrical conductivity reduces the resistance for the electrons at the interface which allows more efficient charge collection. Optimal work function alignment further enhances built-in potential and carrier collection efficiency. Despite Pt's superior efficiency, Au was selected as the optimal back metal owing to its balanced performance, cost-efficiency, and suitability for scalable fabrication processes. The current density-voltage (J-V) curves corresponding to each back metal are detailed in FigThe quantum efficiency vs wavelength (QE-wavelength) corresponding to each back metal are detailed in **Fig**

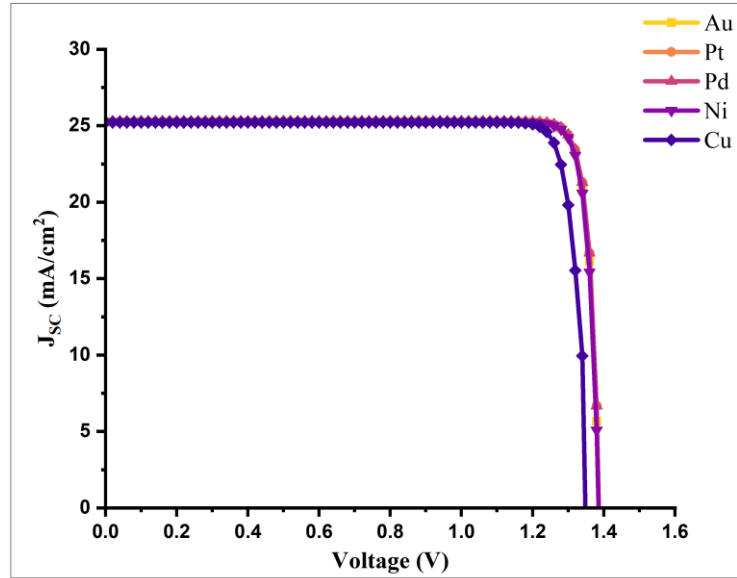


**Figure 4.11:** Graph of  $J_{sc}$  vs Voltage of Different Back Metals with CBTS as HTL and WS2 as ETL.

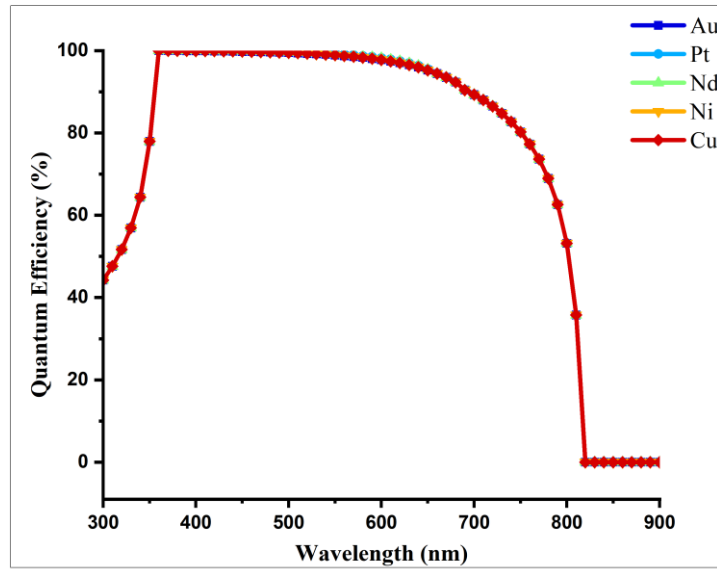


**Figure 4.12:** Graph of QE vs Wavelength of Different Back Metals with CBTS as HTL and WS2 as ETL.

## 4.9 AC characterization

### 4.9.1 Impedance Spectroscopy (IS) measurement

In this segment, we elucidate the Nyquist plots obtained from the Impedance Spectroscopy (IS) analyses conducted on our perovskite solar cell. Nyquist plots visually

depict the complex impedance ( $Z'$ ) across a spectrum of frequencies, represent graphically the real part of the impedance ( $Z'$ ) on the x-axis and imaginary part ( $-Z''$ ) on the y-axis, providing a wealth of information about the charge transport mechanism, interfacial properties and recombination dynamics within the PSCs.

To complement the Nyquist plot analysis, we calculated the conduction band offset (CBO) and the valence band offset (VBO) values for each ETL and HTL combination with the perovskite material. These values of CBO and VBO are mentioned in Table, providing a quantitative assessment of the energy level alignment at the perovskite/ETL and perovskite/HTL interfaces. ETLs with a CBO value close to zero exhibited the best performance, as they minimize the energy barriers for electron and transfer and reduce the recombination losses. Also, HTLs with a small VBO ensured the efficient hole transfer extraction. To facilitate effective hole movement from the light-absorbing layer to the back contact through the HTL, the CBO at the interface between the absorber and the HTL should exhibit a positive value, whereas the VBO should ideally be close to zero or negative. Maintaining a minimal CBO at the ETL/absorber interface is essential to enable smooth and efficient electron transfer from the perovskite layer to the front electrode via the ETL.

$$\Delta E_c = \Delta \chi \quad (4.3)$$

$$\Delta E_v = \Delta E_g - \Delta E_c \quad (4.4)$$

Where,  $\Delta E_g$  is the difference in the bandgap energy and  $\Delta \chi$  is offset in the electron affinities between the materials. [41,42] The optimized electron affinity of  $\text{AgZnF}_3$  is 3.9 eV.

**Table 4.3.** CBO and VBO values For  $\text{AgZnF}_3$ -based Perovskite Solar Cell Interfaces.

Device Structure	CBO	VBO
FTO/ $\text{WS}_2$ / $\text{AgZnF}_3$ / $\text{P}_3\text{HT}$ /Au	-0.05	0.32
FTO/ $\text{TiO}_2$ / $\text{AgZnF}_3$ /CBTS/Au	-0.1	(-1.68)
FTO/PCBM/ $\text{AgZnF}_3$ /CBTS/Au	0	(-0.38)
FTO/ $\text{C}_{60}$ / $\text{AgZnF}_3$ /CBTS/Au	0	(-0.08)
FTO/ $\text{ZnSe}$ / $\text{AgZnF}_3$ /CBTS/Au	-0.19	(-1.38)
FTO/ $\text{CdS}$ / $\text{AgZnF}_3$ /CBTS/Au	-0.5	(-1.3)
FTO/ $\text{WS}_2$ / $\text{AgZnF}_3$ /CBTS/Au	(0.3)	0.02
FTO/ $\text{WS}_2$ / $\text{AgZnF}_3$ / $\text{MoS}_2$ /Au	(0.1)	0.02
FTO/ $\text{WS}_2$ / $\text{AgZnF}_3$ / $\text{Zn}_2\text{P}_3$ /Au	(-0.3)	-0.18
FTO/ $\text{WS}_2$ / $\text{AgZnF}_3$ /MASnBr3/Au	(0.51)	-0.02
FTO/ $\text{WS}_2$ / $\text{AgZnF}_3$ /PEDOT:PSS/Au	(0.5)	0.52

The CBO values for the CBTS, MoS<sub>2</sub>, Zn<sub>2</sub>P<sub>3</sub>, MASnBr<sub>3</sub>, PEDOT: PSS have been determined to be 0.3 eV, 0.1 eV, -0.3 eV, 0.51 eV and 0.5 eV respectively and have been mentioned in parenthesis in CBO. Also, the VBO values for TiO<sub>2</sub>, PCBM, C<sub>60</sub>, ZnSe, CdS have been determined to be -1.68 eV, -0.38 eV, -0.08 eV, -1.38 eV and -1.3 eV respectively and have been mentioned in the parenthesis in VBO.

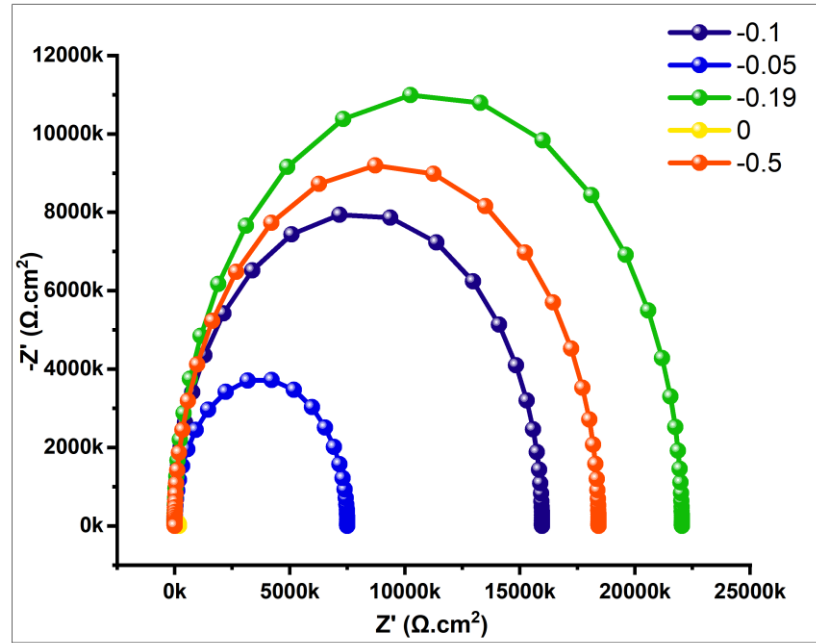


**Figure 4.13:** Nyquist Plot of Impedance Response for AgZnF<sub>3</sub>-based PSC for ETLs with different CBO values.

To gain a comprehensive perspective, we created Nyquist plots for PSC with five different ETLs and three different HTLs. This allowed us to compare the varying ETLs and HTLs impact on the charge transport, recombination, and overall efficiency of the devices. To calculate the Nyquist plots, we configured the optimized perovskite layer incorporating different ETLs and HTLs, along with appropriate contacts. Using the SCAPS-1D Action panel, we initiated the impedance spectroscopy, setting a frequency range of 0 (1.00E-12) Hz to 1 MHz with 100 to 150 logarithmic intervals and executed the simulation to generate the complex impedance data comprising real ( $Z'$ ) and imaginary ( $-Z'$ ) components. We extracted the data to OriginPro, plotting  $Z'$  against  $-Z'$  and enhancing the plot with connecting lines and distinct markers. These plots are semicircular in shape [43]. Semicircular arcs represent the frequency dependent behaviour and insights into the impedance characteristics of charge transport and recombination processes. The high frequency arc in the leftmost side corresponds to the charge transfer resistance at the interface between perovskite and charge transport layer and the low frequency arc in the leftmost side relates to the recombination resistance. A smaller high frequency arc indicates better charge transfer, while a larger low frequency arc refers to less recombination losses. The Nyquist diagrams depicting the CBO are presented in Figure 4.13 and the VBO values are presented in Fig. From Figit is apparent that the semicircular arcs corresponding to CBO of -0.19 eV at the ZnSe/AgZnF<sub>3</sub> junction

exhibits the broader span compared to the other arcs associated with the five different CBO values at the junction. Moreover, Figure 4.14 illustrates that the semicircular curve

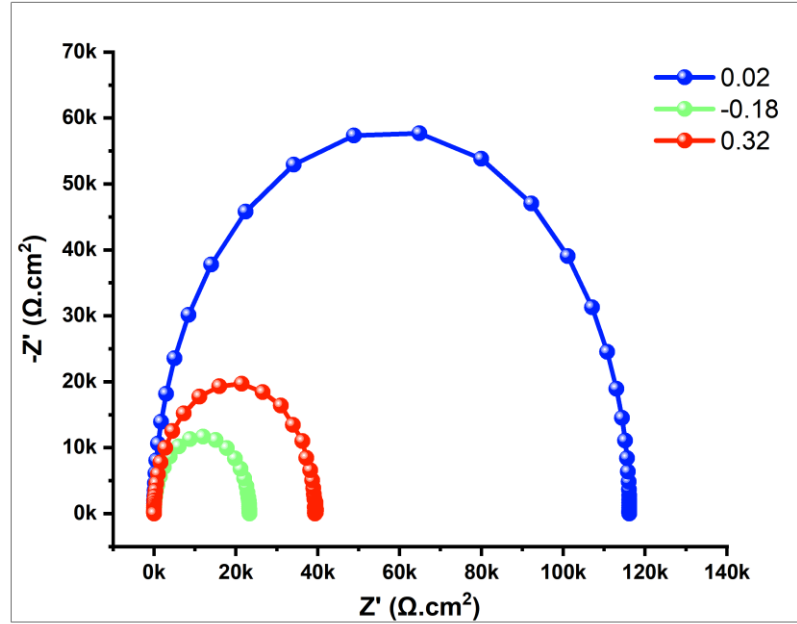


**Figure 4.14:** Nyquist plot of Impedance Response for AgZnF<sub>3</sub>-based PSC for HTLs with different VBO values.

for a VBO of 0.02 eV in the AgZnF<sub>3</sub>-based perovskite solar cell employing MoS<sub>2</sub> as HTL possesses a larger radius than those HTLs namely, Zn<sub>2</sub>P<sub>3</sub> and P<sub>3</sub>HT, which exhibits VBO values of -0.18 eV and 0.32 eV respectively. This is attributed to the proficient transfer of the charge carriers and diminished likelihood of the charge carriers recombination at the ZnSe/AgZnF<sub>3</sub> and AgZnF<sub>3</sub>/MoS<sub>2</sub> interfaces.

## 4.10 Optical Absorption: Absorbance Coefficient vs Photon Energy

The absorption coefficient as a function of photon energy constitutes a pivotal metric in the characterization of optoelectronic materials employed in photovoltaic devices. The absorption coefficient ( $\alpha$ ) quantifies the extent to which a material attenuates incident light per unit thickness, providing insights into the capacity to absorb photons across a range of energies. The absorption coefficient ( $\alpha$ ) delineated the probability of photon absorption within the material, governed by the interplay between the photon energy ( $h\nu$ ) and the bandgap of the material ( $E_g$ ). Photons falling on the material with energies below the bandgap ( $h\nu < E_g$ ) are not able to promote electrons from the valence band to conduction band, thus absorption is negligible. Conversely, as photon energy surpasses the bandgap ( $h\nu \geq E_g$ ), absorption intensifies, reflecting direct and indirect electronics transitions.

The absorption coefficient ( $\alpha$ ) for individual materials within the proposed PSC is calculated using the following equation.[41]



$$\alpha = A_{\alpha} \sqrt{h\nu - E_g} \quad (4.5)$$

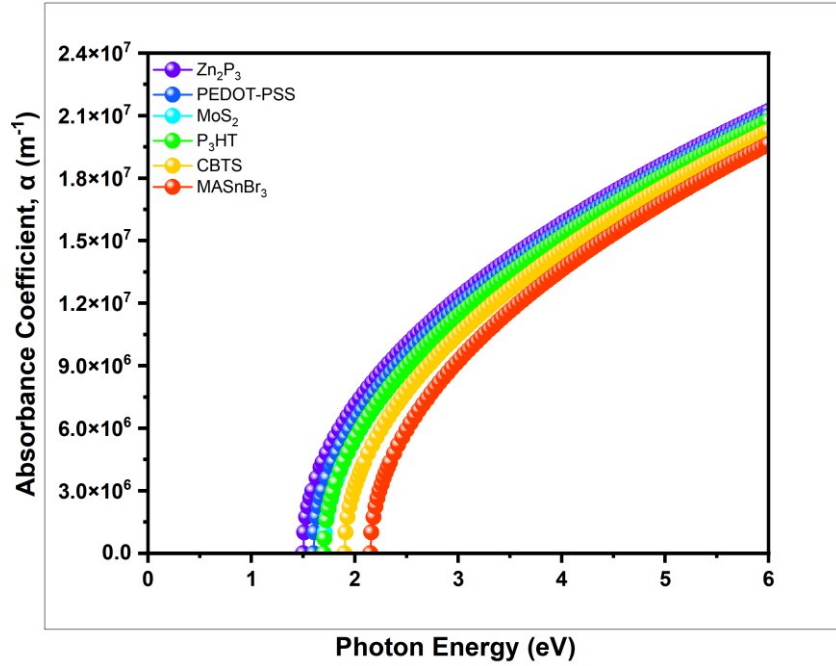


**Figure 4.15:** Variation of Absorption Coefficient with Photon Energy for the Absorber layer and various ETLs.

The energy bandgap ( $E_g$ ) between the valence and conduction band, alongside the energy of impinging photons ( $h\nu$ ) constitutes pivotal variables in the governing equation. The prefatory constant  $A_{\alpha}$  is set at  $10^5 \text{ cm}^{-1} \text{ eV}^{-1/2}$  for all the constituents of the advocated perovskite solar cell structure. The proportion of electromagnetic radiation at a particular wavelength that traverses an element without being ensnared is delineated by the absorption coefficient ( $\alpha$ ). Materials exhibiting high  $\alpha$  value exhibit significantly greater light absorption compared to those with lower  $\alpha$  values [43]. In this investigation, two distinct plots were developed: one representing the absorption coefficient as a function of photon energy for ETLs with the absorber layer, and the other for the HTLs. Fig represents the variation of  $\alpha$  as a function of photon energy for absorber layer and ETLs. The absorption coefficient is plotted on a logarithmic scale ranging from 0 to  $2.3 \times 10^7 \text{ m}^{-1}$ , while the photon energy spans from 0 to 6 eV. The graph shows a distinct trend across all the materials involving a sharp onset of absorption of specific photon energies, followed by a rapid increase in  $\alpha$ , levelling off at higher energies. The behaviour is characteristics of semiconductor, where absorption is negligible for photon energies below the material's  $E_g$  due to the inability of low energy photons to excite the electrons from valence band to conduction band. Among ETLs  $\text{C}_{60}$  and  $\text{WS}_2$  exhibits relatively higher absorption coefficients compared to  $\text{CdS}$  and  $\text{ZnSe}$  which shows the lowest  $\alpha$  values. Among them  $\text{AgZnF}_3$  exhibits the lowest onset energy and the maximum  $\alpha$  (absorption coefficient). Fig represents the variation of absorption coefficient as a function of photon energy for different HTLs. Among HTLs  $\text{Zn}_2\text{P}_3$  shows the highest absorption coefficient compared to  $\text{CBTS}$  and  $\text{MASnBr}_3$  which shows the lowest  $\alpha$

values. The absorption coefficient vs photon energy graph underscores the exceptional light harvesting potential of the AgZnF<sub>3</sub> absorber.

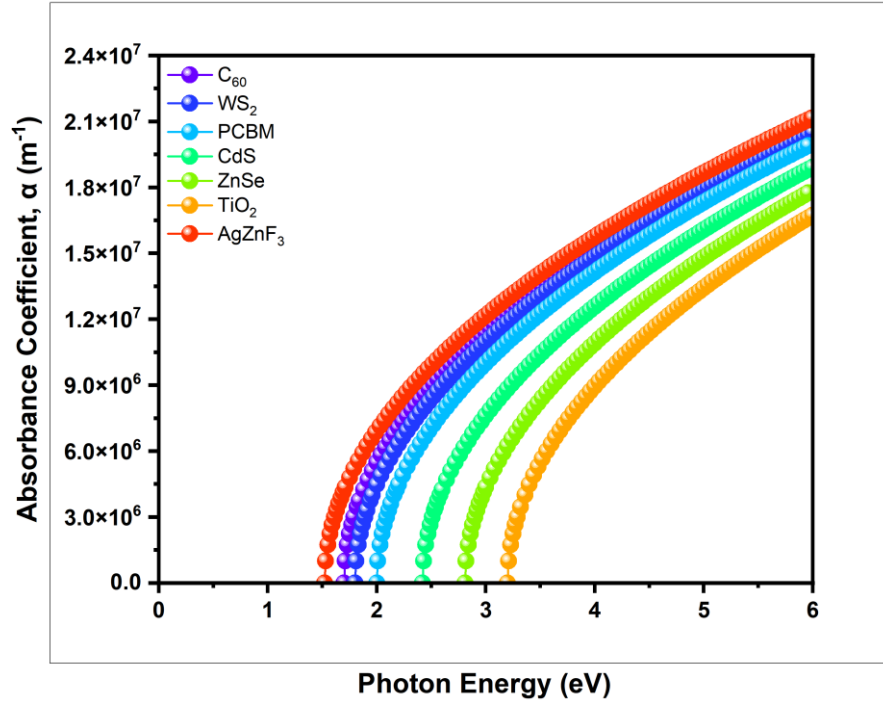


**Figure 4.16:** Variation of Absorption Coefficient with Photon Energy for the various HTLs.

## 4.11 Effect of series resistance

The efficacy of a photovoltaic cell is profoundly influenced by its series resistance ( $R_s$ ), a parameter that quantifies the opposition encountered by electric current as it transverses through multiple layers and interfaces, the buffer layer, the absorber layer, and the metallic contacts. The aggregate resistance, encompassing both the bulk resistance inherent to the material and the resistance attributable to the surface metal contacts, terminals and interconnections, constitutes the principal determinants of the series resistance [44]. To optimize the cell's performance to attain the superior efficiency, it is imperative to minimize the  $R_s$  while maximizing the shunt resistance. However, even under the hypothetical scenario of achieving infinite shunt resistance and the nullifying  $R_s$  [45]. The ramifications of resistive losses can be elucidated through the following equation, derived from the Shockley diode equation, which delineates the interplay between these resistive elements and the overall cell performance [44]. These equations are presented below:

$$I = I_0 \left( e^{\left( \frac{V_j}{nV_0} \right)} - 1 \right) \quad (4.6)$$

Where,  $I$  is the current of the cell with  $I_0$  represents the reverse saturation current,  $n$  representing the identity factor and  $V_j$  and  $V_0$  defines the thermal voltage and diode voltage respectively.

$$I = I_L - I_0 \left( e^{\frac{q(V+IR_s)}{kT}} - 1 \right) - \frac{V + IR_s}{R_{sh}} \quad (4.7)$$

Where,  $q$  is the electron charge and  $k$  is the Boltzmann constant,  $I_L$  defines the light induced current with series resistance  $R_s$ .

$R_s$  predominantly arises from the resistive contributions of the contacts, electrodes as well as the inherent resistivity of the active layer itself [46]. This investigation evaluates the effect of  $R_s$  on the operational characteristics of solar cells employing  $\text{AgZnF}_3$  as absorber material. The  $R_s$  was systematically varied with the range of 0 to 8  $\Omega\text{-cm}^2$  while the shunt resistance is kept constant. The other previous optimized parameters were also maintained constant to isolate and comprehensively analyse the influence of series resistance on the device's performance. In this study,  $R_s$  values ranging from 0 to 8  $\Omega\text{-cm}^2$  have been shown to precipitate substantial declines in PCE and FF. The influence of  $R_s$  on the PV parameters is illustrated in **Fig.** It is observed from the  $J_{sc}$  and  $V_{oc}$  exhibits minimal dependence on the series resistance which can likely be attributed to the absence of substantial increase in recombination losses [47]. As the series resistance increases, a progressive decline in the PCE is observed, dropping from 31.15 to 26.91 %. This

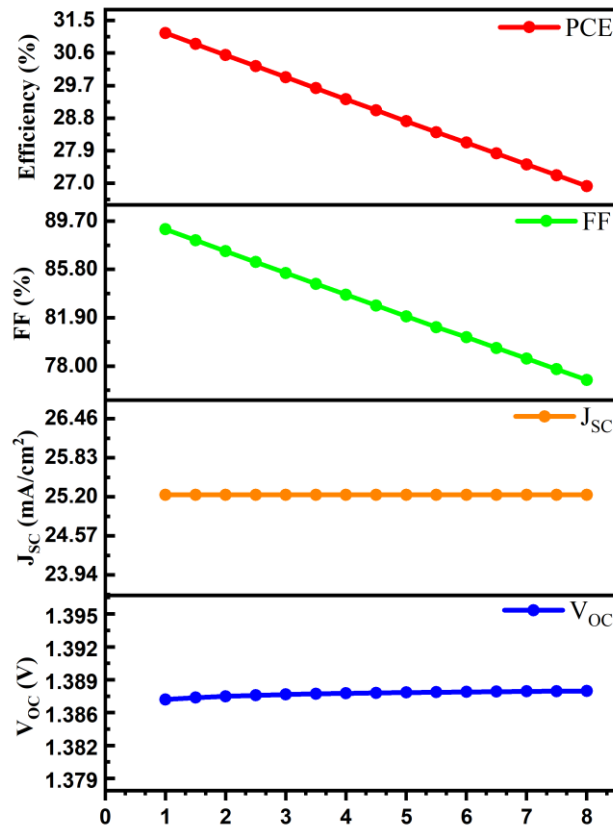


**Figure 4.17:** Effect of Series Resistance on Photovoltaic Performance.

reduction in efficiency is primarily attributed to the increased resistive losses with the device, which hinder the effective extraction of the charge carriers. Similarly, the FF exhibits a significant decrease, falling from 89.03 to 76.88 %, as the elevated series resistance impedes the optimal flow of the current which leading to greater recombination losses. The  $J_{SC}$  also demonstrates a minimal decline, decreasing indicating minimal reduced carrier collection efficiency under higher resistive conditions. In contrast, the  $V_{OC}$  remains relatively stable, with only a slight decrease, as it is predominantly determined by the intrinsic properties of the semiconductor material. For achieving the high-performance photovoltaic cells, it is important to minimizing the  $R_s$ . This can be accomplished through several strategic approaches, such as optimization of the deposition process to decrease the thickness and electrical resistance of the constituent layers. Additionally, enhancing the interfacial quality between the layers and the metallic contacts can improve the charge carrier mobility and mitigate resistive losses. Moreover, decreasing cell's dimension can help minimize the resistance faced by current flow, thereby enhancing the device's overall performance and PCE.

## 4.12 Effect of shunt resistance

The shunt resistance ( $R_{SH}$ ) was systematically varied with the range of  $10^1 \Omega\text{-cm}^2$  to  $10^7 \Omega\text{-cm}^2$  while the series resistance is kept constant in order to examine the effect on the photovoltaic performance.  $R_{SH}$  represents an unintended pathway for the current leakage within the device, which often rising from the imperfections at material interfaces or defects in the semiconductor layers, causing short-circuit the cell and ultimately minimizing the output power [44]. Any current that leaks from the active layer, electrodes or the interface between acceptor and donor materials is a consequence of the shunt resistance [48]. A lower  $R_{SH}$  facilitates increased leakage currents, thereby exacerbating recombination losses and diminishing the overall performance of the device. This phenomenon is particularly evident in the reduction of the  $V_{OC}$ , as a diminished shunt resistance directly correlates with a decline in  $V_{OC}$  and directly affects the photocurrent collected. Consequently, the FF, a critical parameter indicative of the device's efficiency in converting the light into electrical power, is also adversely affected [44], [49]. The influence of  $R_{SH}$  on the PV parameters is illustrated in **Fig**. It is observed that the  $V_{OC}$ , exhibits a significant increase from approximately 0.25232 V at the lowest  $R_{SH}$  value of  $1.38 \text{ V}$  as  $R_{SH}$  approaches to  $10^4 \Omega\text{-cm}^2$ , stabilizing thereafter with minimal variation up to  $10^7 \Omega\text{-cm}^2$ .  $V_{OC}$  is highly sensitive to low  $R_{SH}$  but reaches a plateau once  $R_{SH}$  exceeds a critical threshold. This behaviour is attributed to reduction in recombination losses at the interfaces and within the bulk of the material. Lower  $R_{SH}$  values, increases the current leakage pathways leads to higher recombination rates, which diminish the  $V_{OC}$ . In essence, higher  $R_{SH}$  helps maintain a higher  $V_{OC}$ . The  $J_{SC}$ , remains consistently stable at around  $25.23 \text{ mA/cm}^2$  across the entire  $R_{SH}$  range, indicating that  $J_{SC}$  is largely independent of  $R_{SH}$  variations. In contrast, FF demonstrates a steady rise from approximately 34 % at  $10^1 \Omega\text{-cm}^2$  to 90 % as  $R_{SH}$  increases to  $10^4 \Omega\text{-cm}^2$ , maintaining this elevated level up to  $10^7 \Omega\text{-cm}^2$ . This emphasizes the strong dependence of FF on

$R_{SH}$ , particular at lower values where leakage currents are more evident. Lastly, the PCE, illustrated in blue, increases from 2.18 % at  $10^1 \Omega\text{-cm}^2$  to 31.60 % at  $10^4 \Omega\text{-cm}^2$  and remaining stable thereafter, indicating that PCE is significantly influenced by the  $R_{SH}$ , with optimal performance achieved at higher  $R_{SH}$ . These observations collectively indicate that maintaining a high shunt resistance is crucial for maximizing solar cell's efficiency.

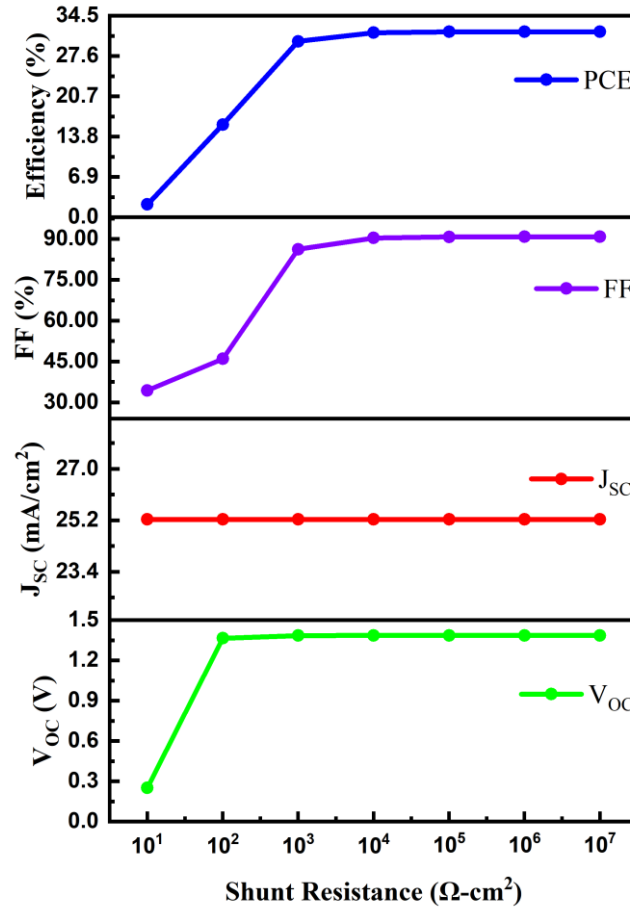


**Figure 4.18:** Effect of Shunt Resistance on Photovoltaic Performance.

### 4.13 Practical insights drawn from simulation results

For practical insights and experimental applications, the stability of the perovskite  $\text{AgZnF}_3$  is very crucial to ensuring its reliability and performance under real-world conditions. At ambient pressure (0 GPa), mechanical stability of cubic  $\text{AgZnF}_3$  and the  $C_{ij}$  (elastic stiffness tensor) value, confirms that  $\text{AgZnF}_3$  is a stable material in the cubic perovskite structure [50]. The useful features of this material can thus be exploited in a significant number of applications due to excellent optical qualities and suitable band gap.  $\text{AgZnF}_3$  possesses a bandgap of 1.52 eV accompanied by notable absorption coefficient, rendering it exceptionally conducive for best performance in perovskite solar cells [18]. Also,  $\text{AgCdF}_3$  is a well-studied perovskite solar cell absorber layer.

Based on these considerations we conducted AgZnF<sub>3</sub> based perovskite solar cell simulations.

The simulated device structure used in this simulation purpose is FTO/WS<sub>2</sub>/AgZnF<sub>3</sub>/CBTS/Au. This device gives us a Power consumption efficiency of 31.77 %, which is remarkably high and thus future research on this device holds significantly potential to yield critical insights that can drive advancements in the realm of the solar cell's technology. The J-V characteristics of FTO/WS<sub>2</sub>/AgZnF<sub>3</sub>/CBTS/Au photovoltaic device, comparing the performance before and after optimization are illustrated in Figure 4.19. The Quantum efficiency (Q.E.) vs wavelength characteristics of the FTO/WS<sub>2</sub>/AgZnF<sub>3</sub>/CBTS/Au PV device, comparing the before and after optimization performance, is detailed in Figure 4.20. The promising efficiency demonstrated by AgZnF<sub>3</sub> holds substantial promise for driving advancements of the solar cell technology. Although, the incorporation of silver (Ag) in AgZnF<sub>3</sub> may results in higher production costs of the device but with the outstanding efficiency of ~ 30% positions the material as a compelling contender for next-generation solar cells.

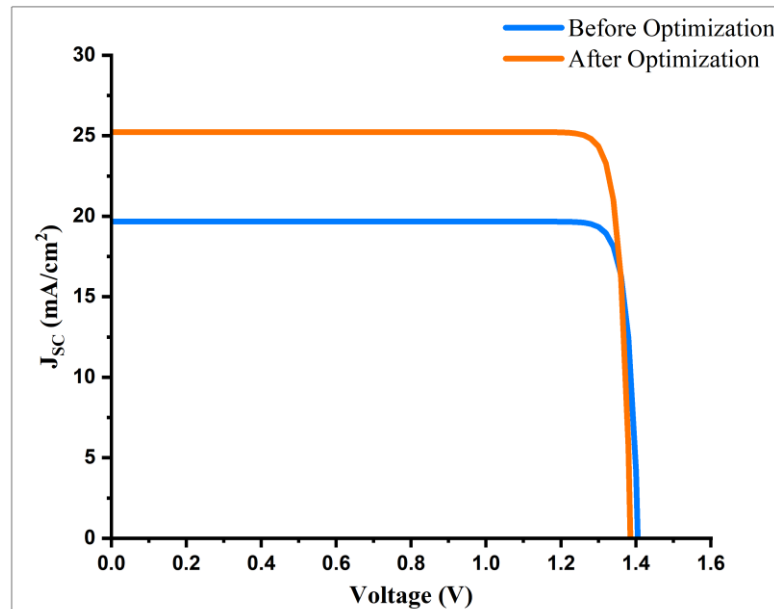


**Figure 4.19:** J-V Characteristics for FTO/WS<sub>2</sub>/AgZnF<sub>3</sub>/CBTS/Au Photovoltaic Device.

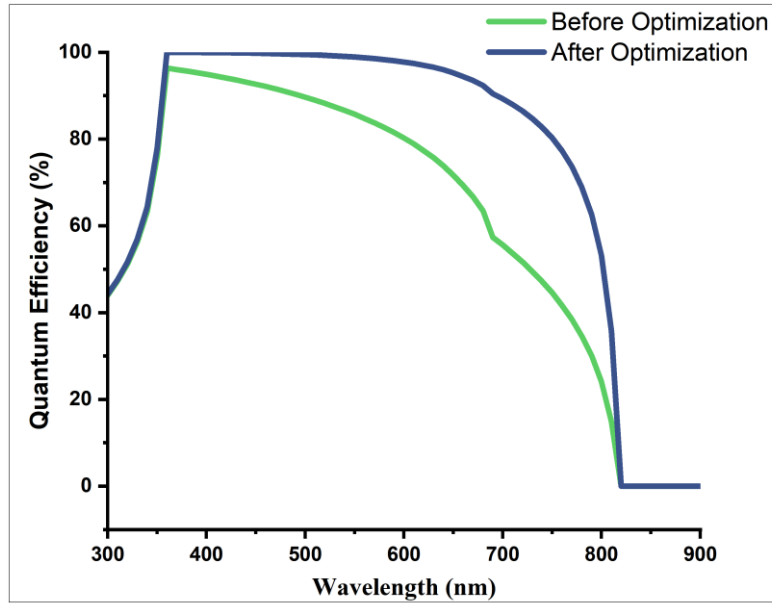


**Figure 4.20:** Q.E. vs Wavelength Characteristics for FTO/WS<sub>2</sub>/AgZnF<sub>3</sub>/CBTS/Au Photovoltaic Device.

#### 4.14 Verification with respect to the ideal Solar cell

An evaluation has been conducted to compare the PV characteristics of AgZnF<sub>3</sub>-based PSCs relative to those of an ideal single junction solar cell, with a focus on the influence of the absorber layer's  $E_g$ . The peak PCE reached an impressive 31.77 %, accompanied by an  $V_{OC}$  of 1.38 V, a  $J_{SC}$  of 25.23 mA/cm<sup>2</sup> and an FF of 90.82 %. The optimal results were achieved with the configuration FTO/WS<sub>2</sub>/AgZnF<sub>3</sub>/CBTS/Au, utilizing an absorber layer of  $E_g$  of 1.52. In contrast, the ideal single junction solar cell exhibits a PCE of 31.00 %, a  $V_{OC}$  of 1.20 V, a  $J_{SC}$  of 29.80 mA/cm<sup>2</sup>, and an FF of 89.90 % at an absorber layer  $E_g$  of 1.50 eV [51]. This highlights that the experimental outcomes of the developed device fall within the performance boundaries of an ideal single junction solar cell.

#### 4.15 Comparison of Simulation and Experimental Results

There is no experimental work on the perovskite material AgZnF<sub>3</sub> till now for the solar cell. However, there is limited direct experimental research work on AgZnF<sub>3</sub> (Argentum Zinc Fluoride) for use in solar cells.

This material is more often studied in the context of photonics, optical properties, and electronic applications.

## 4.16 Challenges and Limitations

**Environmental Stability:**  $\text{AgZnF}_3$  may exhibit different stability characteristics compared to the typical materials used in perovskite solar cells. Perovskites can be sensitive to moisture and oxygen, which can lead to degradation.

**Limited Research:** There is relatively little experimental work or research on the use of  $\text{AgZnF}_3$  in solar cells, especially compared to more established materials like perovskite or silicon. Most research on  $\text{AgZnF}_3$  is focused on its electronic and optical properties for other applications.

**Material Cost:** The raw materials used to make  $\text{AgZnF}_3$  (such as silver and zinc fluoride) may be more expensive or less abundant compared to other photovoltaic materials, such as perovskites or silicon. This could make  $\text{AgZnF}_3$ -based solar cells less economically viable for large-scale production.

**Difficult Synthesis Process:**  $\text{AgZnF}_3$  may be challenging to synthesize in large quantities or with uniform quality. The deposition of high-quality thin films of  $\text{AgZnF}_3$  for use in solar cells may be difficult and expensive due to the material's chemical reactivity, crystallization, and growth conditions.

**Thin Film Deposition:** Thin films of  $\text{AgZnF}_3$  may require special deposition techniques like pulsed laser deposition or sputtering. These techniques could be more complex or costly compared to the solution-processing techniques used to fabricate perovskite solar cells (e.g., spin coating or spray deposition).



# **CHAPTER 5**

## **CONCLUSION**

### **Conclusions**

This study employs numerical modelling via SCAPS-1D software to evaluate and optimize the performance of AgZnF<sub>3</sub> perovskite-based solar cell. The research focuses on simulating the key photovoltaic parameters, including power conversion efficiency (PCE), fill factor (FF), open-circuit voltage (V<sub>oc</sub>), and short-circuit current density (J<sub>sc</sub>) and optimizing device parameters by analysing the impact of different factors. We have comprehensively analysed 8 different HTLs and 6 different ETLs to determine the optimal configuration for augmenting the efficacy and stability of the solar cell. Simulations were centred on perovskite solar cell incorporating silver-based perovskite layer, designed with the layered arrangement FTO/WS<sub>2</sub>/AgZnF<sub>3</sub>/CBTS/Au, where WS<sub>2</sub> and CBTS are electron transport and hole transport materials. Individual device parameter (e.g. thickness, defect density, temperature,) has independently been varied in simulation while holding all other parameters constant. This enabled precise quantification of their influence on the critical performance indicators – power conversion efficiency (PCE), short circuit current density (J<sub>sc</sub>), open circuit voltage (V<sub>oc</sub>) and fill factor (FF). Results deduce that the absorber layer is the principal determinant of device performance, exerting the most significant impact on carrier generation, recombination, charge extraction and thus overall performance of the cell. To assess the effect of the absorber layer, absorber thickness is modulated from the range of 100 nm to 1000 nm, demonstrating a direct correlation between increased thickness and enhanced power conversion efficiency and it becomes maximum at 1000 nm of thickness with a value of 33.40% alongside a fill factor of 90.74%. Conversely, an optimum thickness of 550 nm delivers a balanced PCE of 31.76% accompanied by a notably fill factor of 90.82%. Additionally, the open-circuit voltage was measured at 1.3869 V with the short-circuit current density of 25.214313 mA/cm<sup>2</sup>. The PCE of the solar cell stays consistent up to a defect concentration threshold of 10<sup>10</sup> cm<sup>-3</sup>, after which the performance deteriorates sharply with rising defect concentration. The optimal defect density for sustained efficiency of 31.76% was identified at 10<sup>14</sup> cm<sup>-3</sup>. Through optimization of the electron affinity, systematic variation of absorber layer's electron affinity from 3.4 eV to 4.6 eV revealed optimal band alignment of 3.9 eV, yielding a power conversion efficiency of 31.77% supported by a fill factor of 90.82% with an open-circuit voltage of 1.3862 V and a short-circuit current density of 25.231588 mA/cm<sup>2</sup>. Furthermore, the performance was evaluated across a range of temperatures, confirming the material's stability and efficiency under operational conditions. Across the temperature range of 270K to 380K, the open-circuit voltage decreases steadily from 1.4092 V to 1.3001 V, while the fill factor drops from 91.55% to 88.36%, achieving a highest efficiency of 32.56% at 270 K temperature. The power conversion efficiency falls from 32.56% to 28.98% at 380K temperature. We varied five different back metals and

found platinum (Pt) provided the best results in terms of efficiency (31.86%) and fill factor (90.86%). However, due to high cost of Pt and suitability for scalable fabrication, we opted for gold (Au) because of its balanced performance, which also yielded excellent performance achieving an PV efficiency of 31.77% with a fill factor of 90.82% and an open-circuit voltage of 1.3862 V.

Finally, the optimized PSC structure, FTO/WS<sub>2</sub>/AgZnF<sub>3</sub>/CBTS/Au with the optimized parameters including temperature (300 K), Defect density ( $10^{14} \text{ cm}^{-3}$ ), electron affinity (3.9 eV) and absorber thickness (500 nm) achieved a power conversion efficiency of 31.77% supported by a remarkable fill factor of 90.82%, alongside an open-circuit voltage of 1.3862 V and a short-circuit current density of 25.231588 mA/cm<sup>2</sup>, demonstrating exceptional energy alignment and charge transport.

This study emphasizes the necessity for further exploration and advancement of AgZnF<sub>3</sub>-based perovskite solar cells and highlights the critical need for experimental validation to close the gap between simulation and practical application. While SCAPS-1D model provides a theoretical framework, real- world testing under various environments and operational conditions is imperative to refine the parameters, validate stability ultimately advancing the efficiency and scale production.

## Acknowledgment

The authors are deeply thankful to Marc Burgelman, the Electronics and Information Systems (ELIS) group at the University of Gent, Belgium, for providing us with the SCAPS-1D software.

## REFERENCES:-

- [1] I. Dincer, Renewable energy and sustainable development: a crucial review, n.d. [www.elsevier.com/locate/rser](http://www.elsevier.com/locate/rser).
- [2] W. Chen, M. Alharthi, J. Zhang, I. Khan, The need for energy efficiency and economic prosperity in a sustainable environment, *Gondwana Research* 127 (2024) 22–35. <https://doi.org/10.1016/j.gr.2023.03.025>.
- [3] P. Sadorsky, Renewable energy consumption and income in emerging economies, *Energy Policy* 37 (2009) 4021–4028. <https://doi.org/10.1016/j.enpol.2009.05.003>.
- [4] A.M. Omer, Energy, environment and sustainable development, *Renewable and Sustainable Energy Reviews* 12 (2008) 2265–2300. <https://doi.org/10.1016/j.rser.2007.05.001>.
- [5] T.Y. Lin, Y. ho Chiu, C.H. Chen, L. Ji, Renewable energy consumption efficiency, greenhouse gas emission efficiency, and climate change in Europe, *Geoenergy Science and Engineering* 247 (2025). <https://doi.org/10.1016/j.geoen.2025.213665>.
- [6] K. Alanne, A. Saari, Distributed energy generation and sustainable development, *Renewable and Sustainable Energy Reviews* 10 (2006) 539–558. <https://doi.org/10.1016/j.rser.2004.11.004>.
- [7] N. Kannan, D. Vakeesan, Solar energy for future world: - A review, *Renewable and Sustainable Energy Reviews* 62 (2016) 1092–1105. <https://doi.org/10.1016/j.rser.2016.05.022>.
- [8] N.G. Park, Perovskite solar cells: An emerging photovoltaic technology, *Materials Today* 18 (2015) 65–72. <https://doi.org/10.1016/j.mattod.2014.07.007>.
- [9] C. Yang, W. Hu, J. Liu, C. Han, Q. Gao, A. Mei, Y. Zhou, F. Guo, H. Han, Achievements, challenges, and future prospects for industrialization of perovskite solar cells, *Light Sci Appl* 13 (2024). <https://doi.org/10.1038/s41377-024-01461-x>.
- [10] W. Ke, C.C. Stoumpos, M.G. Kanatzidis, “Unleaded” Perovskites: Status Quo and Future Prospects of Tin-Based Perovskite Solar Cells, *Advanced Materials* 31 (2019) 1803230. <https://doi.org/10.1002/ADMA.201803230>.
- [11] S. Lee, J. Ryu, D.G. Lee, P. Pandey, C.M. Oh, I.W. Hwang, S.W. Cho, S. Yoon, J.Y. Lee, D.W. Kang, Unprecedented inorganic HTL-based MA-free Sn–Pb perovskite photovoltaics with an efficiency over 23%, *Energy Environ Sci* 17 (2024) 8140–8150. <https://doi.org/10.1039/D4EE03579H>.
- [12] Deepika, A. Singh, U.K. Verma, S. Ameen, Optimization of lead-free materials-based perovskite solar cell using SCAPS-1D simulation, *Journal of Physics and Chemistry of Solids* 186 (2024). <https://doi.org/10.1016/j.jpcs.2023.111817>.
- [13] E.W.G. Diau, E. Jokar, M. Rameez, Strategies to improve performance and stability for tin-based perovskite solar cells, *ACS Energy Lett* 4 (2019) 1930–1937.

[https://doi.org/10.1021/ACSENERGYLETT.9B01179/ASSET/IMAGES/MEDIUM/NZ-2019-011796\\_0005.GIF](https://doi.org/10.1021/ACSENERGYLETT.9B01179/ASSET/IMAGES/MEDIUM/NZ-2019-011796_0005.GIF).

- [14] U.U. Rehman, R.S. Almufarij, A.R. Abd-Elwahed, K.U. Sahar, E. Hussain, A. Ashfaq, K. Mahmood, C.M. Wang, Improving efficiency of germanium-based perovskite solar cells with graphene interface layer: A strategy to minimize charge recombination, *Journal of Physics and Chemistry of Solids* 198 (2025) 112487. <https://doi.org/10.1016/J.JPCS.2024.112487>.
- [15] L. Chen, H. Cai, X. Luo, X. Zhao, S. Wu, Modifying the buried PEDOT:PSS/perovskite interface by dual-functional material to optimize the performance of pure Sn-based Perovskite Solar Cells, *Surfaces and Interfaces* 57 (2025). <https://doi.org/10.1016/j.surfin.2025.105743>.
- [16] H. Sharma, V.K. Verma, R.C. Singh, P.K. Singh, A. Basak, Numerical Analysis of High-Efficiency CH<sub>3</sub>NH<sub>3</sub>PbI<sub>3</sub> Perovskite Solar Cell with PEDOT:PSS Hole Transport Material Using SCAPS 1D Simulator, *J Electron Mater* 52 (2023) 4338–4350. <https://doi.org/10.1007/S11664-023-10257-5/METRICS>.
- [17] A.M.N. ABENA, A.T. NGOUPO, F.X.A. ABEGA, J.M.B. NDJAKA, Numerical investigation of solar cells based on hybrid organic cation perovskite with inorganic HTL via SCAPS-1D, *Chinese Journal of Physics* 76 (2022) 94–109. <https://doi.org/10.1016/j.cjph.2021.12.024>.
- [18] A. Abbas, M.B. Tahir, B. Ahmed, M. Sagir, A. Dahshan, H.E. Ali, Insight on Cu-doping dependent structural, electronic and optical properties of AgZnF<sub>3</sub> Fluro-perovskite for solar cell applications: A DFT study, *Optik (Stuttg)* 304 (2024). <https://doi.org/10.1016/j.ijleo.2024.171717>.
- [19] H.L. Sun, C.L. Yang, M.S. Wang, X.G. Ma, Y.G. Yi, High thermoelectric efficiency fluoride perovskite materials of AgMF<sub>3</sub> (M = Zn, Cd), *Mater Today Energy* 19 (2021). <https://doi.org/10.1016/j.mtener.2020.100611>.
- [20] F.T. Zahra, M.M. Hasan, M.B. Hossen, M.R. Islam, Deep insights into the optoelectronic properties of AgCdF<sub>3</sub>-based perovskite solar cell using the combination of DFT and SCAPS-1D simulation, *Heliyon* 10 (2024). <https://doi.org/10.1016/j.heliyon.2024.e33096>.
- [21] G. Murtaza, G. Sadique, H.A. Rahnamaye Aliabad, M.N. Khalid, S. Naeem, A. Afaq, B. Amin, I. Ahmad, First principle study of cubic perovskites: AgTF<sub>3</sub> (T=Mg, Zn), *Physica B Condens Matter* 406 (2011) 4584–4589. <https://doi.org/10.1016/j.physb.2011.09.026>.
- [22] M.K. Hossain, G.F.I. Toki, D.P. Samajdar, M. Mushtaq, M.H.K. Rubel, R. Pandey, J. Madan, M.K.A. Mohammed, M.R. Islam, M.F. Rahman, H. Bencherif, Deep Insights into the Coupled Optoelectronic and Photovoltaic Analysis of Lead-Free CsSnI<sub>3</sub> Perovskite-Based Solar Cell Using DFT Calculations and SCAPS-1D Simulations, *ACS Omega* 8 (2023) 22466–22485. <https://doi.org/10.1021/acsomega.3c00306>.
- [23] M.F. Rahman, M.M. Alam Moon, M.K. Hossain, M.H. Ali, M.D. Haque, A. Kuddus, J. Hossain, A.B. Abu, Concurrent investigation of antimony chalcogenide (Sb<sub>2</sub>Se<sub>3</sub> and Sb<sub>2</sub>S<sub>3</sub>)-based solar cells with a potential WS<sub>2</sub> electron transport layer, *Heliyon* 8 (2022). <https://doi.org/10.1016/j.heliyon.2022.e12034>.

- [24] H. Bencherif, M. Khalid Hossain, Design and numerical investigation of efficient (FAPbI<sub>3</sub>)<sub>1-x</sub>(CsSnI<sub>3</sub>)<sub>x</sub> perovskite solar cell with optimized performances, *Solar Energy* 248 (2022) 137–148. <https://doi.org/10.1016/j.solener.2022.11.012>.
- [25] A.A. Kanoun, M.B. Kanoun, A.E. Merad, S. Goumri-Said, Toward development of high-performance perovskite solar cells based on CH<sub>3</sub>NH<sub>3</sub>GeI<sub>3</sub> using computational approach, *Solar Energy* 182 (2019) 237–244. <https://doi.org/10.1016/j.solener.2019.02.041>.
- [26] A. Tara, V. Bharti, S. Sharma, R. Gupta, Computational approach to explore suitable charge transport layers for all inorganic CsGeI<sub>3</sub> perovskite solar cells, *Opt Mater (Amst)* 128 (2022). <https://doi.org/10.1016/j.optmat.2022.112403>.
- [27] M.U. Alam, Md.K.I. Shifat, J.K. Modak, Md. Tarekuzzaman, Md.I. Haque, Md. Rasheduzzaman, M.A. Qader, R. Islam, Y. Arafat, Md.Z. Hasan, Improving the efficiency and performance of Rb<sub>2</sub>SnI<sub>6</sub>-based perovskite solar cells through comprehensive optimization: A numerical study, (2024). <https://doi.org/10.21203/rs.3.rs-5364684/v1>.
- [28] V. Deswal, S. Kaushik, R. Kundara, S. Baghel, Numerical simulation of highly efficient Cs<sub>2</sub>AgInBr<sub>6</sub>-based double perovskite solar cell using SCAPS 1-D, *Materials Science and Engineering: B* 299 (2024). <https://doi.org/10.1016/j.mseb.2023.117041>.
- [29] S. Sani, A. Usman, A. Bhatranand, Y. Jiraraksopakun, K.S. Muhammad, U. Yahaya, A study on defect, doping, and performance of ETLs (ZnO, TiO<sub>2</sub>, and IGZO) for the lead-free CsSnCl<sub>3</sub> perovskite solar cell by SCAPS-1D framework, *Mater Today Commun* 38 (2024). <https://doi.org/10.1016/j.mtcomm.2023.107575>.
- [30] M.M. Rahman, M.H. Ali, M.D. Haque, A.Z.M. Touhidul Islam, Numerical modeling and extensive analysis of an extremely efficient RbGeI<sub>3</sub>-based perovskite solar cell by incorporating a variety of ETL and HTL materials to enhance PV performance, *Energy Advances* (2024). <https://doi.org/10.1039/d4ya00323c>.
- [31] M.Q. Kareem, S.A. Hassan, S.S. Alimardan, S.M. Shareef, M.M. Ameen, CHTS/Zn<sub>2</sub>P<sub>3</sub>-based solar cells with enhanced efficiency through ETL engineering: A numerical study, *Journal of Physics and Chemistry of Solids* 188 (2024). <https://doi.org/10.1016/j.jpcs.2024.111931>.
- [32] R.F.. Pierret, *Semiconductor device fundamentals*, (2008) 792. [https://books.google.com/books/about/Semiconductor\\_Device\\_Fundamentals.html?id=P-VNfYbs3r0C](https://books.google.com/books/about/Semiconductor_Device_Fundamentals.html?id=P-VNfYbs3r0C) (accessed January 30, 2025).
- [33] M.Y. Toriyama, A.M. Ganose, M. Dylla, S. Anand, J. Park, M.K. Brod, J.M. Munro, K.A. Persson, A. Jain, G.J. Snyder, How to analyse a density of states, *Materials Today Electronics* 1 (2022). <https://doi.org/10.1016/j.mtelec.2022.100002>.
- [34] A. Abbas, M.B. Tahir, B. Ahmed, M. Sagir, A. Dahshan, H.E. Ali, Insight on Cu-doping dependent structural, electronic and optical properties of AgZnF<sub>3</sub> Fluro-perovskite for solar cell applications: A DFT study, *Optik (Stuttg)* 304 (2024). <https://doi.org/10.1016/j.ijleo.2024.171717>.
- [35] P. Sawicka-Chudy, Z. Starowicz, G. Wiesz, R. Yavorskyi, Z. Zapukhlyak, M. Bester, Głowa, M. Sibiński, M. Cholewa, Simulation of TiO<sub>2</sub>/CuO solar cells with SCAPS-1D software, *Mater Res Express* 6 (2019) 085918. <https://doi.org/10.1088/2053-1591/AB22AA>.

- [36] N.K. Sinha, D.S. Ghosh, A. Khare, Role of built-in potential over ETL/perovskite interface on the performance of HTL-free perovskite solar cells, *Opt Mater (Amst)* 129 (2022) 112517. <https://doi.org/10.1016/J.OPTMAT.2022.112517>.
- [37] P. Holzhey, M. Saliba, A full overview of international standards assessing the long-term stability of perovskite solar cells, *J Mater Chem A Mater* 6 (2018) 21794–21808. <https://doi.org/10.1039/C8TA06950F>.
- [38] R. Roesch, T. Faber, E. Von Hauff, T.M. Brown, M. Lira-Cantu, H. Hoppe, Procedures and Practices for Evaluating Thin-Film Solar Cell Stability, *Adv Energy Mater* 5 (2015) 1501407. <https://doi.org/10.1002/AENM.201501407>.
- [39] H. Baig, H. Kanda, A.M. Asiri, M.K. Nazeeruddin, T. Mallick, Increasing efficiency of perovskite solar cells using low concentrating photovoltaic systems, *Sustain Energy Fuels* 4 (2020) 528–537. <https://doi.org/10.1039/C9SE00550A>.
- [40] K. Deepthi Jayan, V. Sebastian, Comprehensive device modelling and performance analysis of MASnI<sub>3</sub> based perovskite solar cells with diverse ETM, HTM and back metal contacts, *Solar Energy* 217 (2021) 40–48. <https://doi.org/10.1016/J.SOLENER.2021.01.058>.
- [41] T.M. Khan, B. Islam, M.M. Rahaman, M. Md Shakil, M.F. Rahman, S.R. Al Ahmed, Predictive design and performance analysis of lead-free CH<sub>3</sub>NH<sub>3</sub>SnI<sub>3</sub>-based perovskite solar cells through a combination of SCAPS-1D and machine learning based modelling, *Solar Energy Materials and Solar Cells* 282 (2025). <https://doi.org/10.1016/j.solmat.2024.113388>.
- [42] T.A. Dar, A. Agrawal, P. Misra, L.M. Kukreja, P.K. Sen, P. Sen, Valence and conduction band offset measurements in Ni<sub>0.07</sub>Zn<sub>0.93</sub>O/ZnO heterostructure, *Current Applied Physics* 14 (2014) 171–175. <https://doi.org/10.1016/j.cap.2013.10.017>.
- [43] K. Sekar, L. Marasamy, S. Mayarambakam, P. Selvarajan, J. Bouclé, Highly efficient lead-free silver bismuth iodide (Ag<sub>3</sub>BiI<sub>6</sub>) rudorffite solar cells with novel device architecture: A numerical study, *Mater Today Commun* 38 (2024). <https://doi.org/10.1016/j.mtcomm.2024.108347>.
- [44] Md.S. Uddin, R. Hosen, S. Sikder, H. Mamur, M.R.A. Bhuiyan, Photovoltaic performance enhancement of Al/ZnO:Al/i-ZnO/CdS/CIGS/Pt solar cell using SCAPS-1D software, *Next Energy* 2 (2024) 100080. <https://doi.org/10.1016/j.nxener.2023.100080>.
- [45] J.H. Kim, D. Shin, B.T. Ahn, Surface morphology control of In<sub>2</sub>S<sub>3</sub> buffer layer by Sn incorporation and its application to cadmium-free Cu(In,Ga)Se<sub>2</sub> thin-film solar cells, *Current Applied Physics* 16 (2016) 1040–1045. <https://doi.org/10.1016/J.CAP.2016.06.004>.
- [46] M. Islam, T. Ahmed, S.U.D. Shamim, A.A. Piya, A. Basak, Thickness dependent numerical investigations of lead free perovskite/CIGS bilayer solar cell using SCAPS-1D, *Chemistry of Inorganic Materials* 2 (2024) 100034. <https://doi.org/10.1016/j.cinorg.2024.100034>.
- [47] E.L. Meyer, S. Jakalase, A. Nqombolo, N. Rono, M.A. Agoro, The Numerical Simulation of a Non-Fullerene Thin-Film Organic Solar Cell with Cu<sub>2</sub>FeSnS<sub>4</sub> (CFTS) Kesterite as a

Hole Transport Layer Using SCAPS-1D, *Coatings* 15 (2025) 266.  
<https://doi.org/10.3390/coatings15030266>.

- [48] K.I.F. Utsho, S.M.G. Mostafa, M. Tarekuzzaman, M.S.M. Al-Saleem, N.I. Nahid, J.Y. Al-Humaidi, M. Rasheduzzaman, M.M. Rahman, M.Z. Hasan, Optimizing Cs<sub>2</sub>CuBiBr<sub>6</sub> double halide perovskite for solar applications: the role of electron transport layers in SCAPS-1D simulations, *RSC Adv* 15 (2025) 2184–2204.  
<https://doi.org/10.1039/d4ra08515a>.
- [49] S. Karthick, S. Velumani, J. Bouclé, Experimental and SCAPS simulated formamidinium perovskite solar cells: A comparison of device performance, *Solar Energy* 205 (2020) 349–357. <https://doi.org/10.1016/j.solener.2020.05.041>.
- [50] S. Hiadsi, H. Bouafia, B. Sahli, B. Abidri, A. Bouaza, A. Akriche, Structural, mechanical, electronic and thermal properties of KZnF<sub>3</sub> and AgZnF<sub>3</sub> Perovskites: FP-(L)APW+lo calculations, *Solid State Sci* 58 (2016) 1–13.  
<https://doi.org/10.1016/j.solidstatesciences.2016.05.005>.
- [51] A. Morales-Acevedo, Fundamentals of solar cell physics revisited: Common pitfalls when reporting calculated and measured photocurrent density, open-circuit voltage, and efficiency of solar cells, *Solar Energy* 262 (2023).  
<https://doi.org/10.1016/j.solener.2023.05.051>.

# NISHANT HOODA

## Dissertation final Repo nishant rt.docx

 Delhi Technological University

---

### Document Details

Submission ID

trn:oid::27535:99855009

Submission Date

Jun 8, 2025, 4:10 PM GMT+5:30

Download Date

Jun 8, 2025, 4:13 PM GMT+5:30

File Name

Dissertation final Repo nishant rt.docx

File Size

3.0 MB

45 Pages

10,704 Words

60,007 Characters







# 6% Overall Similarity

The combined total of all matches, including overlapping sources, for each database.




## Filtered from the Report

- Bibliography
- Quoted Text
- Cited Text
- Small Matches (less than 8 words)

## Match Groups

-  **75 Not Cited or Quoted 6%**  
Matches with neither in-text citation nor quotation marks
-  **0 Missing Quotations 0%**  
Matches that are still very similar to source material
-  **0 Missing Citation 0%**  
Matches that have quotation marks, but no in-text citation
-  **0 Cited and Quoted 0%**  
Matches with in-text citation present, but no quotation marks

## Top Sources

- 2%  Internet sources
- 3%  Publications
- 4%  Submitted works (Student Papers)

## Integrity Flags

### 0 Integrity Flags for Review

No suspicious text manipulations found.

Our system's algorithms look deeply at a document for any inconsistencies that would set it apart from a normal submission. If we notice something strange, we flag it for you to review.

A Flag is not necessarily an indicator of a problem. However, we'd recommend you focus your attention there for further review.

## Match Groups

- 75 Not Cited or Quoted 6%**  
Matches with neither in-text citation nor quotation marks
- 0 Missing Quotations 0%**  
Matches that are still very similar to source material
- 0 Missing Citation 0%**  
Matches that have quotation marks, but no in-text citation
- 0 Cited and Quoted 0%**  
Matches with in-text citation present, but no quotation marks

## Top Sources

- 2% Internet sources
- 3% Publications
- 4% Submitted works (Student Papers)

## Top Sources

The sources with the highest number of matches within the submission. Overlapping sources will not be displayed.

- 1** **Publication**  
Fatema-Tuz- Zahra, Md Mehidi Hasan, Md. Bokhtiar Hossen, Md. Rasidul Islam. "D... <1%
- 2** **Submitted works**  
George Bush High School on 2023-05-24 <1%
- 3** **Internet**  
worldwidescience.org <1%
- 4** **Internet**  
riunet.upv.es <1%
- 5** **Internet**  
thesis.univ-biskra.dz <1%
- 6** **Submitted works**  
Higher Education Commission Pakistan on 2023-06-01 <1%
- 7** **Internet**  
scaps.elis.ugent.be <1%
- 8** **Submitted works**  
The University of Manchester on 2017-09-03 <1%
- 9** **Submitted works**  
Mawlana Bhashani Science and Technology University on 2024-02-15 <1%
- 10** **Submitted works**  
Maulana Azad National Institute of Technology Bhopal on 2021-04-02 <1%

11	Submitted works	University of Wales Swansea on 2021-05-21	<1%
12	Submitted works	University of Newcastle upon Tyne on 2025-05-23	<1%
13	Publication	Hajar Benali, Bouchaib Hartiti, Fatima Lmai, Abdelkrim Batan, Salah Fadili, Philipp...	<1%
14	Internet	d-nb.info	<1%
15	Publication	Eri Widiyanto, Shobih, Eryta Septa Rosa, Kuwat Triyana, Natalita Maulani Nursam...	<1%
16	Publication	Ahmed Abbas, Muhammad Bilal Tahir, Bilal Ahmed, M. Sagir, A. Dahshan, H. Elhos...	<1%
17	Submitted works	Higher Education Commission Pakistan on 2025-03-06	<1%
18	Submitted works	King's College on 2012-12-14	<1%
19	Submitted works	Sheffield Hallam University on 2013-02-13	<1%
20	Internet	efiling.energy.ca.gov	<1%
21	Internet	patents.google.com	<1%
22	Submitted works	American University of the Middle East on 2022-05-15	<1%
23	Publication	Ashok Adhikari, Jorge Evaristo Conde Diaz, Odin Reyes-Vallejo, Francisco Javier Gó...	<1%
24	Publication	Ashok Adhikari, Odin Reyes Vallejo, Jorge Evaristo Conde Diaz, Jacobo Martinez-R...	<1%

25	Publication	Biswajit Pal, Abhijeet J. Kale, Minakshi Sharma, K. C. Bhamu, Sung Gu Kang, Vijay ...	<1%
26	Publication	J. Prince Allen Jebakumar, D. Jackuline Moni, D. Gracia, M. Daphny Shallet. "Desig...	<1%
27	Submitted works	Loughborough University on 2019-09-06	<1%
28	Publication	Neelima Singh, Mohit Agarwal. "Numerical insights of lead-free manganese-base...	<1%
29	Submitted works	Sheffield Hallam University on 2017-03-28	<1%
30	Publication	Simya, O.K., A. Mahaboobbatcha, and K. Balachander. "A comparative study on th...	<1%
31	Submitted works	Universiti Kebangsaan Malaysia on 2023-08-17	<1%
32	Submitted works	University of Sheffield on 2020-05-01	<1%
33	Submitted works	VIT University on 2022-10-11	<1%
34	Submitted works	Cornell University on 2021-01-04	<1%
35	Submitted works	Deakin University on 2018-10-02	<1%
36	Submitted works	Gulf University on 2015-10-03	<1%
37	Submitted works	Islamic University of Technology on 2025-06-02	<1%
38	Publication	Jack Arayro, Rabih Mezher, Hussein Sabbah. "Comparative Simulation Study of th...	<1%

39	Publication	Nishant Rana, Jignasa V. Gohel. "Metal-organic frameworks for enhanced perfor...	<1%
40	Publication	Shahram Rafiee Rafat, Zahra Ahangari, Mohammad Mahdi Ahadian, Seied Ali Hos...	<1%
41	Publication	Shazia Akhtar Dar, Basharat Want, Brajendra Singh Sengar. "Enhancing efficiency...	<1%
42	Publication	Sheikh Rashel Al Ahmed. " Investigation on the Performance Enhancement of Het...	<1%
43	Submitted works	University of Bristol on 2013-02-05	<1%
44	Submitted works	University of Durham on 2018-04-18	<1%
45	Submitted works	Walailak University: The Center for Library Resources and Educational Media on 2...	<1%
46	Submitted works	Xiamen University on 2023-12-08	<1%
47	Internet	cwww.intechopen.com	<1%
48	Internet	hdl.handle.net	<1%
49	Internet	link.springer.com	<1%
50	Internet	ntnuopen.ntnu.no	<1%
51	Internet	repositorium.uminho.pt	<1%
52	Internet	www.hofstra.edu	<1%

53

Internet

www.mdpi.com

<1%

